pubs.acs.org/FF Article

A Model-Based Assessment of the Added Values of Hydroprocessed Esters and Fatty Acids-Synthetic Paraffinic Kerosene Blends on Aircraft Performance, Emissions, and Safety

Published as part of Energy & Fuels special issue "18th International Conference on Stability, Handling and Use of Liquid Fuels (IASH2024)".

Stephan Ruoff,* Georg Eckel, Uwe Bauder, Patrick Le Clercq, and Manfred Aigner



Cite This: Energy Fuels 2025, 39, 16968-16984

energysfuels



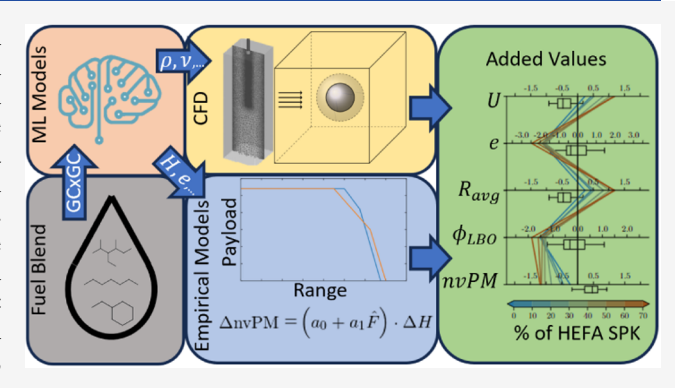
ACCESS

III Metrics & More

Article Recommendations

Supporting Information

ABSTRACT: The aviation industry tries to reduce its carbon footprint by shifting toward sustainable aviation fuel (SAF). With the increasing proportion of SAF in the fuel mix, careful consideration must be given to mitigating any safety risks while realizing its full benefits. In this context, this study presents a comprehensive framework for assessing safety aspects together with the added values of SAF on aircraft performance and emissions. The framework enables the prediction of various performance metrics using composition-based property models and empirical correlations. A key aspect of this research is the systematic propagation of uncertainties inherent in the property prediction models and correlations. To illustrate the framework's capabilities, two fuels representing the spectrum of conventional jet fuels were



blended with hydroprocessed esters and fatty acids-synthetic paraffinic kerosene (HEFA-SPK) synthetic blend component (SBC) at various ratios. These blends were compared to a reference fuel, and the range of conventional fuels documented in the Coordinating Research Council (CRC) world fuel survey. The results indicate that the selected SBC can improve aircraft performance through enhanced specific energy (energy per unit mass). Additionally, the study reveals that HEFA-SPK can substantially reduce emissions, particularly nvPM, and thereby mitigate contrail-induced radiative forcing. However, the study also points out that safety-related properties, such as density and aromatic content, constrain higher blending ratios. Additionally, the study evaluates different modeling approaches for predicting soot emissions and LBO, revealing potential limitations in the existing models. The findings underscore the importance of a multimetric approach for fuel assessment. This work aims to provide a foundation for informed decision making in the development and implementation of SAF, ultimately contributing to the industry's sustainability goals.

1. INTRODUCTION

In response to the pressing challenges of climate change, the European Union has implemented the "Fit for 55" package, aimed at reducing greenhouse gas (GHG) emissions by at least 55% by 2030. One key component of this package is the ReFuelEU Aviation Initiative, which specifically addresses the aviation sector's contribution to the climate. It introduces a broad framework for the implementation of SAF. The core element is the SAF blending mandate, which requires fuel suppliers to incorporate minimum shares of sustainable synthetic blend components (SBCs), starting with a 2% requirement in 2025, increasing to 70% by 2050 (Figure 1). A certain percentage (35% in 2050) has to come from renewable fuels of nonbiological origin (RFNBO), which are fuels produced from renewable energy sources, hydrogen and CO₂. In this context, SAFs are fuels that are more sustainable

than traditional kerosene, whereas SBCs refer to neat synthetic fuels produced from one of the approved production pathways defined in the ASTM D7566³ annexes, with an emphasis on their technical viability rather than their environmental sustainability. The US set a SAF production target of 3 billion gallons by 2030 and 35 billion gallons by 2050 in the SAF Grand Challenge.⁴ With the total jet fuel uplift of 23 billion gallons in 2019 expected to grow to about 34 billion gallons by

Received: June 18, 2025 Revised: August 13, 2025 Accepted: August 14, 2025 Published: August 20, 2025





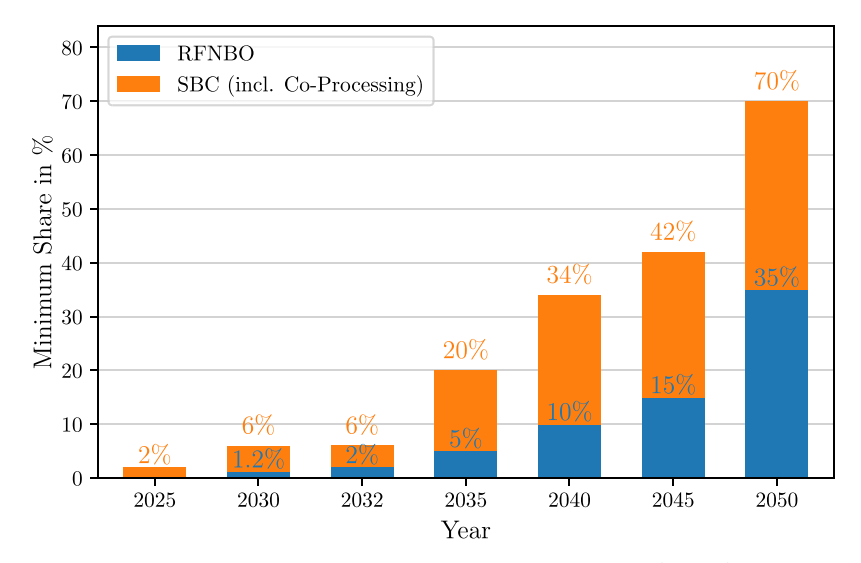


Figure 1. Minimum shares in ReFuelEU Aviation's SAF blending mandate. Of the total SBCs (orange), a certain percentage has to stem from renewable fuels of nonbiological origin (RFNBO).²

2050,⁵ the targets correspond to 10 and 100% of the jet fuel demand, respectively.

The primary goal is the reduction of CO_2 throughout the entire life cycle of the fuel, from feedstock sourcing and processing to transportation and use. Beyond the CO_2 reduction, SAF offers additional environmental and economic benefits. These so-called "added values" include significant reductions in particulate emissions, mitigating contrail formation as well as increasing the efficiency of aircraft. In this regard, the recent in-flight measurements of the Emission and Climate Impact of Alternative Fuel (ECLIF) campaigns together with modeling efforts further improved the understanding of aviation's climate impact and the impact of fuel composition on these effects. $^{8-11}$

The rapid development of new production pathways for SBCs necessitates fast and efficient methods to evaluate their potential benefits and impacts on performance, emissions, and safety. While traditional approaches such as experimental testing in original hardware offer high accuracy, they are often too time-consuming and expensive. The adoption of machine learning models can significantly accelerate the assessment process ¹² and was successfully implemented in the fuel prescreening. ¹³ Building on these capabilities, optimization methodologies have been developed, enhancing fuel performance characteristics ^{14,15} or SAF yield. ¹⁶

Nevertheless, most recent advancements focus on one single aspect within the broad landscape impacted by the fuel. However, focusing on improving one metric (e.g., the volumetric energy density), might overlook or impair another metric (e.g., the sooting tendency). 17 Furthermore, the impact on more complex processes, such as lean blowout (LBO) or contrail formation, is difficult to estimate from the data available, which are typically the properties measured for ASTM D7566³ certification. Therefore, this study introduces a comprehensive tool to simultaneously assess the impact of novel fuels on various metrics regarding safety (density at 15 °C, distillation slopes $(T_{90} - T_{10})$ and $T_{50} - T_{10}$, kinematic viscosity at -40 °C, aromatic content, derived cetane number (DCN) and LBO), as well as performance (volumetric and gravimetric energy density, aircraft range for a given payload, fuel uptake for a given mission) and emissions (CO₂, H₂O₂ nonvolatile particulate matter (nvPM), mass-based yield

sooting index (YSI_m) , contrails and effective radiative forcing (ERF)).

One critical aspect of fuel assessment is the proper consideration of uncertainties by systematic uncertainty quantification (UQ) to enable well-informed decision making. For composition-based property predictions, uncertainties have been addressed using competing models, ¹⁸ probabilistic frameworks, ¹⁹ or predictive capability metrics. ²⁰

Building on the recent advances in fuel modeling and the effort in understanding the influence of SAF on aircraft performance and emissions, this study introduces a list of metrics to assess the added value of SAF. Using state-of-the-art, fuel-sensitive, composition-based property models alongside both established and novel empirical correlations, a framework to predict the metrics was developed. One focus was the propagation of uncertainties that arise from the property prediction models but also from the correlations themselves. To display the novel approach, two fuels representing the range of conventional jet fuels, as well as blends in various ratios with a HEFA-SPK are compared to a reference fuel and the range of experience in conventional fuels represented by the Coordinating Research Council (CRC) world fuel survey.²¹ Furthermore, this study also compares different modeling approaches for soot and LBO prediction, which may indicate potential limitations within the models themselves.

2. METRICS FOR THE FUEL ASSESSMENT

2.1. Safety. Safety is the number one priority in aviation, where the reliability of aircraft systems and the safety of passengers depend on strict standards and procedures. As the industry shifts toward using novel fuels, it is essential to maintain the high safety standards that have been established for conventional jet fuels. Key fuel properties are reflected in the American Society for Testing and Materials (ASTM) fuel specifications, ^{3,22} which a fuel must meet to become certified for usage in a commercial flight. This study uses a reduced subset of those properties to illustrate the methodology, but its scope can be easily expanded to accommodate any additional properties as needed. During the transition to 100% SBC, blended fuels will play a crucial role. In this context, Zschocke²³ carried out an extensive study using various jet

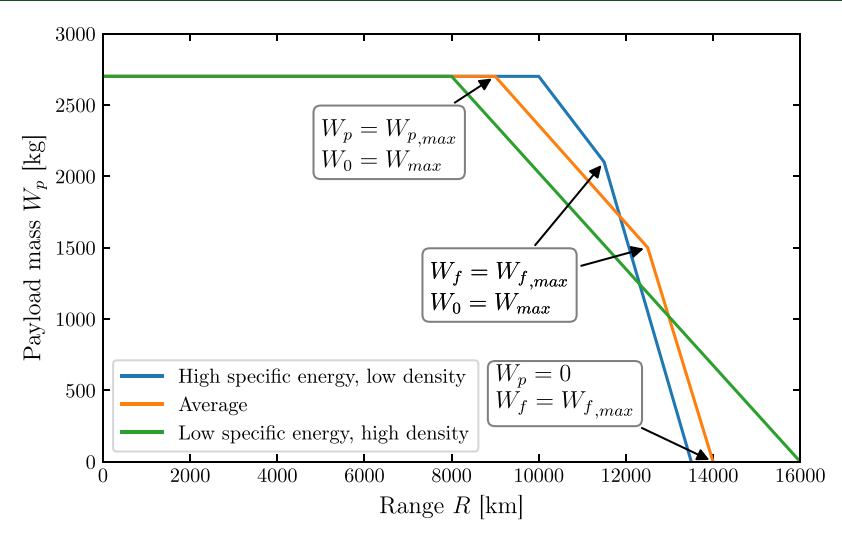


Figure 2. Payload-range diagram for typical business jet.²⁹ Different colors illustrate different fuels: one average fuel, one with a higher density and lower gravimetric energy density (specific energy), and one with a lower density and higher specific energy than the average jet fuel.

fuels, alternative fuels, and blends thereof. They identified the density (at 15 °C), distillation slopes ($T_{90}-T_{10}$ and $T_{50}-T_{10}$), low-temperature kinematic viscosity (at -40 °C), and aromatic content as important properties to be monitored when blending synthetic with conventional fuels.

Density is a safety-related metric, since many other fuel properties, such as dielectric constant or heat capacity, scale directly with the density. 24,25 According to the US Department of Defense,²⁴ the dielectric constant is of importance, since aircrafts "utilize capacitance probes in their tanks to measure the fuel level". The distillation slope was introduced in reaction to the bad altitude relight performance of South African Synthetic Oil Limited (Sasol)'s fully synthetic jet fuel (FSJF).^{26,27} De Klerk²⁸ notes that it is also included to avoid too narrow distillation cuts and to ensure smooth vaporization during continuous combustion. The kinematic viscosity is highly relevant for the operability of fuel pumps as well as fuel nozzles and the atomization process needed for combustion. Since the viscosity is inversely proportional to temperature, it is critical at low temperatures. The aromatic content, even though influencing the hydrogen mass content of the fuel H_f and thus emissions and energy content of the fuel, is also first and foremost a safety-relevant metric. Nitrile rubber O-rings, although no longer the preferred choice, have been widely used as seals in legacy aircraft systems and can still be found in many existing fleets. The swelling of these seals is sensitive to the aromatic content of the fuel and can lead to leakage in the aircraft fuel system.

In addition to the properties mentioned by Zschocke, this study also expands the methodology to include properties that affect combustor operability, namely, LBO and DCN (which influences the LBO behavior), highlighting the importance of considering key parameters that are not part of the traditional fuel specifications but can still have a major impact on system behavior.

- **2.2. Performance.** The assessment focuses on performance metrics that affect operational efficiency, specifically the fuel's range and payload (PL) capacity, to evaluate its effectiveness in supporting flights over varying distances and different payloads.
- 2.2.1. Range and Payload. To determine the range and payload capacity of an aircraft, the energy content of jet fuel

plays a crucial role. It refers to the amount of energy released per unit mass or unit volume of fuel when it is burned. The range R refers to the maximum distance an aircraft can travel on a given mass of fuel W_p while the payload weight W_p refers to the weight of passengers, cargo, and other items that an aircraft can carry. The takeoff weight W_0 is the sum of the empty weight W_e , the payload weight W_p , and the fuel weight W_a

The trade-off between payload and range is illustrated by a payload-range diagram, as given in Figure 2. The curve can be divided into three sections, separated by abrupt changes in slope. The top horizontal line represents the maximum payload, where the range is extended by adding more fuel until the maximal structural weight $W_{\rm max}$ of the airframe is reached ($W_0 = W_{\rm max}$ first kink). Thus, to further increase the range R, the payload has to be traded for more fuel. The second kink in the curve represents the point where the maximum amount of fuel ($W_f = W_{f,\rm max}$) is reached, which is limited by the volume of the fuel tanks. To further increase the range, the payload has to be reduced, leading to the aircraft operating below its maximum structural weight ($W_0 < W_{\rm max}$). The maximum range is thus the distance that an aircraft can fly without carrying any payload ($W_p = 0$).

2.2.2. Flight Mission Metric. The metrics to determine whether a fuel performs better than another are based on scenarios introduced by Kosir et al. ¹⁴ The first scenario describes the maximum range (in kilometers) an aircraft can fly for a given payload in (passengers or cargo)

$$R_{\max,p} = \max(R|W_p = SP) \tag{1}$$

The specific payload SP is the percentage of available seating or payload capacity that is actually being used.

The second scenario describes the amount of fuel (in kilograms) needed for a typical mission with a given specific payload and specific range $W_{f_{R_p}}$

$$W_{f_{R,p}} = (W_f | R = SR \wedge W_p = SP)$$
(2)

This study investigates three flight missions: two flight missions based on the first scenario and one flight mission based on the second. The data for the flights and payloads are taken from the Department of Transportation's Bureau of Transportation Statistics database.³⁰ The most frequently used

Energy & Fuels pubs.acs.org/EF Article

aircraft in the period from 2011 to 2022, the Boeing 737–300-CFM561B1, was selected. The first two flight missions target the $R_{\max,p}$ for a given payload. The first case specifies the $R_{\max,p}$ at the mean payload percentage for the 737–300 in that period of time of SP = 66.12%. The second case is specified as an "empty" aircraft, with an SP = 20%. The third case, in contrast, calculates the fuel uptake for the aircraft going the most frequent route in the period (HOU–DAL), which corresponds to a distance of 239 mi and the same payload percentage as the first case.

2.3. Emissions. Emissions in the aviation sector are of critical importance for the environment and society due to their impact on local air quality, climate, and health. Aircraft emissions consist mainly of water H_2O and carbon dioxide CO_2 . Additionally, there are products from the incomplete combustion, such as unburnt hydrocarbons (UHC), carbon monoxide (CO), and nonvolatile particulate matter (nvPM) (including soot). Further, sulfur present in the fuel (up to 3000 ppm according to ASTM D1655²²) and nitrogen contained in the ambient air can react to sulfur oxides (SO_x) and nitrogen oxides (SO_x), respectively.

The emission indices (EIs) provide a standardized way to compare emissions across different aircraft types, engine models, operational conditions, or fuel compositions. The mass emission index (EI_m) is the mass of the pollutants emitted by an aircraft engine per fuel mass burned. In contrast to the EI_m , the number emission index (EI_n) quantifies the number of particles per kilogram of fuel emitted.

The climate impact of emissions can be quantified by the ERF, which describes the extent to which emissions alter the Earth's energy balance, i.e., the net radiative flux between incoming solar radiation, the Earth's surface, and the atmospheric system.³¹ A positive ERF implies a warming, and a negative one implies a cooling impact on the climate. The review of Lee et al.³¹ compiled results and analyzed the possible contribution of the aviation sector on the effective radiative forcing compared to preindustrial times. In Table 1,

Table 1. Net Effective Radiative Forcing Terms and CIs from Lee et al.³¹ for Selected Components^a

component	ERF ± 95% CI	reference EI	EI unit
CO_2	$34.3^{+\ 5.7}_{-6.3}$	$3.16 \cdot 10^3$	g/(kg fuel)
H_2O	$2.0^{+\ 1.2}_{-1.2}$	$1.231 \cdot 10^3$	g/(kg fuel)
NO_x	$17.5^{+11.5}_{-16.9}$	15.14	g/(kg fuel)
$soot^b$	$0.94^{+\ 3.06}_{-0.84}$	$1.225 \cdot 10^{15}$	#/(kg fuel)
contrail cirrus	$57.4^{+0.6}_{-40.4}$		
SO_x^c	$-7.4^{+4.8}_{-11.6}$	1.2	g/(kg fuel)

^aReference emission indices taken representing the average emission indices for the year 2018. ^bThis study, discussed in Table 2. ^cAssumed $Y_S = 600$ ppm.

an excerpt of the data is shown and later used to determine the climate impact of a given fuel. The modeling and calculation of the ERF in this study are discussed in Sections 3.2.2 and 3.2.3. The cause and magnitude of the uncertainties can be understood by categorizing the emission effects into three main groups: direct GHG emissions (e.g., CO_2 , H_2O), emissions influencing other GHGs (e.g., NO_x , SO_x), and emissions that have an impact on cloud formation and associated climate effects (e.g., soot). Emissions with a more direct impact on radiative forcing tend to have smaller

uncertainty ranges. For more information, the reader is referred to Lee et al.³¹

2.3.1. Particle Emissions (Soot). Particulate emissions at the engine exhaust consist mainly of ultrafine soot or black carbon emissions and are called nonvolatile particulate matter (nvPM). They have a typical geometric diameter of 15 to 60 nm³² and contribute to adverse health and climate impacts. The nvPM can be characterized in different ways. The smoke number (SN) was introduced by the International Civil Aviation Organization (ICAO) in 1981. Measurement involves collecting soot particles on a filter and assessing the resulting accumulation. As only particles larger than 300 nm³³ are sampled, it does not directly address health impacts. Therefore, standards for nvPM were developed to replace it. One of them is the mass concentration nvPM (nvPM EI,), which was established by the Committee on Aviation Environmental Protection (CAEP) of the ICAO.³⁴ With the CAEP/11,³⁵ the number nvPM (nvPM EI,) was added, and was also adopted by the European Union Aviation Safety Agency (EASA). A different measure to quantify the sooting tendency of a fuel is the yield sooting index (YSI), which was introduced by McEnally and Pfefferle in ref 36. They suggest that other concepts like the smoke point (already part of the ASTM D7566³ specifications) or the threshold sooting index (TSI)³⁷ have a higher uncertainty than the YSI. Furthermore, the available TSI data is not yet extensive enough to facilitate the development of a robust machine learning model, despite the efforts of Boehm, Zhibin, and Heyne³⁸ in measuring TSI for various compounds.

Even though particle emissions only make up a very small portion of the total emissions of aircraft, they have a large impact on the climate and the aircraft system itself. For soot particles, the direct impact of its aerosol-radiation is small (cf. Table 1). However, emitted soot particles interact with the water vapor (from ambient air and coemitted) and eventually form contrail cirrus clouds. The water rapidly condenses onto the soot particles, and as the engine exhaust plume cools down, it freezes to form line-shaped contrails. The formation process and persistence of the contrails strongly depend on the ambient conditions (temperature, water content). In ice supersaturated regions, the contrails sustain for hours or days and will lose their linear shape as they transition into contrail cirrus.³⁹ In terms of soot, the "reduction of soot number emissions leads to a lower initial ice crystal number concentration at contrail formation because of the decrease in the number of available condensation nuclei". 40 Thus, the nvPM EI, is a better indicator for ice crystal and contrail formation (and eventually the climate impact) than the nvPM

With respect to the aircraft's engine itself, soot also has a negative influence. It can lead to blockage of small orifices (e.g., dilution holes, atomizer),⁴¹ increased heat load on liners, reduced combustor efficiency, increased nonsoot emissions,⁴² and poorer combustion stability.⁴³

2.3.2. Gaseous Emissions. There are different mechanisms that cause gaseous emissions in the combustion of jet fuels. The (ideal) complete combustion of hydrocarbons (generic jet fuel (C_xH_y)) can be expressed by the global reaction equation

$$C_x H_y + \left(x + \frac{y}{4}\right) O_2 \rightarrow x C O_2 + \frac{y}{2} H_2 O$$
 (3)

It states that the amounts of CO_2 and H_2O emitted solely depend on the hydrogen-to-carbon ratio (H/C) of the fuel and

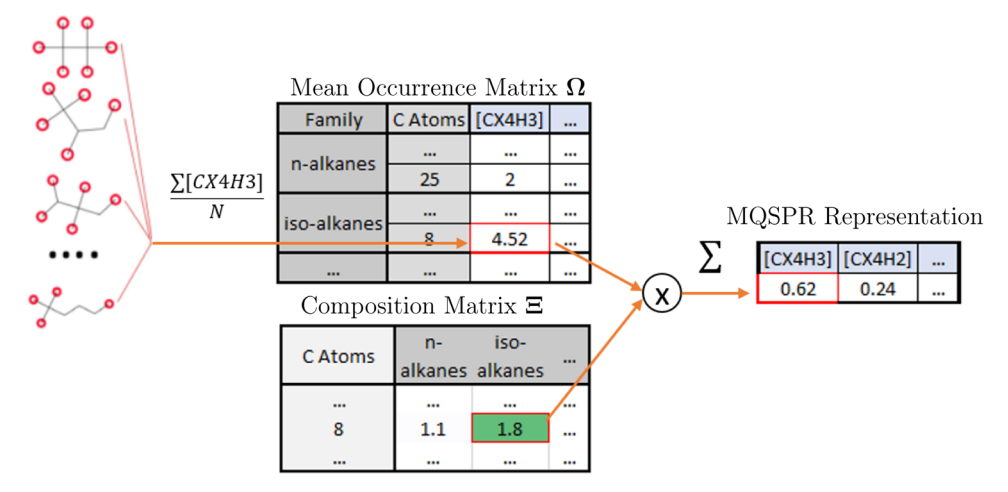


Figure 3. Schematic of the estimation of the MQSPR representation of a jet fuel using GCxGC measurement matrix Ξ and mean occurrence matrix Ω^{53} .

Ξ	n- alkanes	iso- alkanes	 P	n- alkanes	iso- alkanes	 Σ	n- alkanes	iso- alkanes	
C Atoms	~~~	┴ ~	 C Atoms	~~~	↓ ~	 C Atoms	~~~	┴ ~	
7	0.0	0.0	 7	688	693	 7	0.0	8.2	
8	1.1	1.8	 8	706	714	 8	0.0	10.5	
9	2.4	5.8	 9	722	725	 9	0.0	13.3	
10	2.0	5.7	 10	735	746	 10	0.0	14.0	
11	2.3	6.4	 11	743	766	 11	0.0	13.7	
17	0.0	1.1	 17	777	804	 17	0.0	18.1	
18	0.0	0.1	 18	778	814	 18	0.0	19.2	

Figure 4. Schematic of mean matrix model with composition matrix Ξ (left), mean property matrix P (middle), and standard deviation matrix Σ (right). The exemplary values represent the density at 15 °C.

the amount of fuel that is burned. Incomplete combustion can additionally lead to the release of harmful emissions, including carbon monoxide (CO) and unburned hydrocarbons (UHC). Moreover, a typical jet fuel is not free of any contaminants; it can also contain sulfur. The sulfur in the fuel also reacts with oxygen and can form sulfur dioxide (SO₂), sulfur trioxide (SO_3) , or even sulfuric acid (H_2SO_4) . SO_x are further oxidized to form sulfate particles, resulting in a negative ERF.³¹ Lastly, Nitrogen oxides (NOx), which include nitrogen monoxide (NO) and nitrogen dioxide (NO₂), are formed during the combustion of fuels in air. There are three primary mechanisms through which NO_x is formed during aircraft engine combustion: thermal NO_x, prompt NO_x, and fuel NO_x. Since prompt and thermal NO_x are the dominant formation processes, it can be stated that the NO_x EI is heavily dependent on the combustor design and operating conditions and less on the fuel.⁴⁴ Aviation NO_x emissions contribute to climate change by increasing tropospheric ozone (O₃) (warming effect) and reducing methane (cooling effect). However, due to the complexity of interactions of NO_x in the atmosphere, "the net effect of aircraft engine NO_x emissions on ERF remains uncertain".31

3. FUEL-SENSITIVE MODELING

Modeling the performance of jet fuels is challenging due to the large number of parameters and the diverse range of fuel properties that must be considered. To address this complexity, a hybrid approach is developed. For direct fuel properties, such as density or viscosity, where extensive data sets are available, machine learning models are utilized. In contrast, for properties where fuel-dependent data is scarce, but the physical mechanisms are well understood, empirical or semiempirical formulas are applied.

3.1. Machine Learning Model. Aviation fuels consist of several hundreds of different hydrocarbon molecules, which influence their properties. Using data from fuel databases such as the NIST Standard Reference Database, ⁴⁵ DIPPR 801, ⁴⁶ PubChem, ⁴⁷ ChemSpider, ⁴⁸ and the DLR SimFuel-database, machine learning models are trained. The models take different kinds of information on the fuel, e.g., the molecular structure of its molecules or a composition measured by two-dimensional (2D) gas chromatography (GCxGC), to predict its properties (e.g., density ρ , viscosity ν).

3.1.1. Mean Quantitative Structure—Property Relationship. Most of the properties used in this paper are calculated using the Mean quantitative structure—property relationship (MQSPR) model, ¹⁹ which is based on the work of Ajmani et al. ⁴⁹ The basic concept of the model is to correlate the structure of a molecule with its physicochemical properties using a quantitative structure—property relationship (QSPR) approach. ^{50–52} The structure itself is approximated by quantifying molecular descriptors, such as the carbon number or the number of methyl groups. For each molecule in the databases, the relevant properties are calculated and provide

Energy & Fuels pubs.acs.org/EF Article

the foundation for the calculation of the MQSPR model for complex fuels.

In the MQSPR model, each jet fuel is modeled as an entity using its GCxGC composition matrix (Ξ), resulting in a moleaveraged quantitative pseudo-structure. This structure is described by 49 structural features, which are also used in the QSPR method. This enables the model training to use both pure compound data and data from real fuels. For each property, a mean occurrence matrix Ω is created, which includes the 49 structural features for all possible isomers of a fuel family at a given carbon number. The precalculated mean occurrence matrix is then multiplied with the molar fractions of the GCxGC measurements of the fuels to determine the QSPR representation of the fuel, which is then used as an input to the QSPR model f to predict the desired property

$$\psi_{\text{mix}} = f \left(\sum_{i,j} \Xi_{i,j} \cdot \Omega_{i,j} \right) \tag{4}$$

A schematic illustration is given in Figure 3.

3.1.2. Mean Matrix Model. For the calculation of the distillation and YSI, the mean matrix model, depicted in Figure 4. is utilized

$$\psi_{\text{mix}} = \sum_{i,j} \mathbf{\Xi}_{i,j} \cdot \mathbf{P}_{i,j} \quad \text{PI}(\psi_{\text{mix}}) = \sum_{i,j} \mathbf{\Xi}_{i,j} \cdot (\mathbf{P}_{i,j} \pm \Sigma_{i,j})$$
(5)

As for the MQSPR model, the composition matrix Ξ represents the composition of the fuel based on GCxGC measurements. The properties, in contrast to the MQSPR model, are stored in two matrices: the mean property matrix P and the standard deviation matrix Σ. Contrary to the MQSPR model, each cell in P corresponds to the average property for a given hydrocarbon family with a given carbon number. The properties are calculated in advance, sampled from measurements in the databases or predicted using the QSPR approach. Finally, the mean and standard deviation for each cell in the matrix are calculated. The standard deviation matrix is later used to propagate the uncertainties using prediction intervals (PIs) (eq 5, right side), which is also an integral component of our fuel prescreening framework.

The Mean Matrix model was preferred over the MQSPR model for the following reasons: Modeling the distillation with the MQSPR model, only fuel data (e.g., no molecular data) can be used for the correlation, since single molecules only have a boiling point, but no in-between distillation points such as T_{10} or T_{50} . This effectively reduces it to a direct correlation method. With the limited GCxGC data available compared to pure compounds, this can lead to overfitting and restrict extrapolation to fuels not in the training data. The Mean Matrix model, in contrast, uses the isomers in each cell and calculates from their boiling point distribution how much volume of each bin is already evaporated at a given temperature. From these data, the distillation curve is computed. For the YSI, the accuracy of the MQSPR prediction depends strongly on whether the compounds used to create the mean occurrence matrix Ω are present in the fuel, since the isomeric variance of the YSI is significant.⁵⁴ Moreover, there were no data available for fuels and mixtures during the model training, which is why an extrapolation to complex fuels leads to high uncertainties. The mean matrix model uses a linear mixing rule, as proposed by Das et al.,55 for the different

isomers available in each cell, which is better suited for extrapolating to different multicomponent fuels.

3.2. Empirical Models. 3.2.1. Correlations for Range, Payload, and Consumed Fuel. When the range and payload capabilities of different fuels are compared, the key parameters are the volumetric energy density U and the gravimetric energy density e (also denoted specific energy). The lower calorific value of the fuel LCV, also often referred to as net heat of combustion, is the amount of energy released per unit mass, when a fuel is combusted and the water vapor in the combustion products remains in gaseous form. It is typically given in MJ/kg and thus equivalent to the gravimetric energy density e. In contrast, the volumetric energy density is the amount of energy per unit volume (MJ/m³) and can be calculated as $U = e \cdot \rho$.

To depict the influence of changes in volumetric and gravimetric energy density, two lines were added to Figure 2. The blue line represents a fuel with a higher gravimetric energy density but lower density than an average fuel. For this fuel, the first kink moves slightly to the right, since the same amount of fuel mass carries more energy and thus extends the range for maximum payload $(W_p = W_{p,\max})$. Due to its lower density, however, the maximum amount of fuel is lower $(W_{f,\max} = \rho_f V_f)$, leading to a lower overall range compared to the average fuel.

The green line portrays a fuel with higher density but lower gravimetric energy density, which results in an overall higher volumetric energy density. Due to the lower gravimetric energy density, the maximum range is lower for $W_p = W_{p,\max}$. It also leads to the fact that there is no second kink, since the high density and thus fuel weight make it impossible to fill the tank completely $(W_f < W_{f,\max})$ when a payload is carried $(W_p > 0)$ in order not to exceed the maximum weight W_{\max} . Instead, the overall maximum range of the aircraft $(W_p = 0)$ is extended.

To summarize, a higher gravimetric energy density *e* leads to higher ranges with full payload but can affect the maximum range. As the density increases, the range can be extended to a certain degree, but payload might have to be sacrificed. As noted in Blakey et al., ²⁹ commercial aircraft tend to be flown close to the maximum payload, and therefore a light fuel with high gravimetric energy density is preferred. High-density fuels, in contrast, are more appropriate for flight missions where the maximum range is of prime interest.

The calculation of the maximum range for a given payload $R_{\max,p}$ and estimation of the fuel weight for a given range and payload $W_{f_{R,p}}$ is based on the so-called Breguet range equation. The makes the assumption that the aircraft is already in straight and level flight (i.e., at cruise), flying at a true air speed u and with full fuel tanks. In this horizontal flight, there is a balance between the thrust and the drag, as well as the aircraft weight and lift. Thus, the range can be estimated by

$$R = \frac{u \cdot L/D}{g \cdot c_{\mathrm{T}}} \cdot \ln \left(\frac{W_{1}}{W_{2}} \right) = \frac{u \cdot L/D}{g \cdot c_{\mathrm{T}}} \cdot \ln \left(\frac{W_{0}}{W_{0} - W_{f}} \right) \tag{6}$$

where $c_{\rm T}$ is the thrust specific fuel consumption, L/D is the Lift-to-Drag ratio, and W_1 is the aircraft weight at the start and W_2 at the end of the flight cycle. For a given fuel weight W_f and takeoff weight $W_0 = W_e + W_p + W_f$, it translates to the expression on the right side.

To take into account the effects of different fuels, it is expected that during cruise, the combustion efficiency and therefore the thrust and heat release of the combustion will Energy & Fuels pubs.acs.org/EF Article

remain constant. This can be incorporated into eq 6 by adjusting c_T of a given fuel i according to

$$c_{T_i} = c_{T_{\text{ref}}} \frac{\text{LCV}_{\text{ref}}}{\text{LCV}_i} \tag{7}$$

where LCV_{ref} = 43.2 MJ/kg is the 20-year average LCV of kerosene within the U.K., taken from Snijders and Melkert, ⁵⁷ and $c_{T_{\rm ref}}$ is the corresponding thrust specific fuel consumption for the aforementioned average in a given aircraft.

3.2.2. Correlations for Emissions. Aviation emissions depend on a range of variables, encompassing the aircraft and engine used, atmospheric conditions, and flight mission profile. Incorporating the influence of aviation fuel introduces another level of complexity. To estimate the emissions for the different fuel compositions, the following correlations identified in the literature or derived from physical and chemical equations are employed.

3.2.2.1. nvPM (Soot). SAF effects on nvPM EI $_n$ were investigated over a large range of engine thrust settings during, among others, the second Emission and Climate Impact of Alternative Fuel (ECLIF-II) campaign. During the campaign, Voigt et al. observed a correlation between H_f and the nvPM EI $_n$ and also the ice particle number (N_{ice}). Teoh et al. used the measurements of the campaign to extend the methodology of Brem et al. (first part of eq 8). The correlation is based on the arithmetic difference of H_f (ΔH) with respect to a conventional fuel with $H_{f,ref}$ = 13.8%. However, the linear approach leads to unrealistic nvPM reductions of more than 100% for ΔH > 0.6%. Thus, the second part in eq 8 was introduced to give the correlation an asymptotic behavior toward a 100% reduction in nvPM, which was validated for ΔH < 1.1%

$$\Delta \text{nvPMEI}_n \% = \begin{cases} (a_0 + a_1 \hat{F}) \cdot \Delta H, & \text{if } \Delta H \leq 0.5 \\ (a_0 + a_1 \hat{F}) \cdot \Delta H \cdot \exp\left(\frac{0.5 - \Delta H}{2}\right), & \\ & \text{if } \Delta H > 0.5 \end{cases} \tag{8}$$

with $a_0 = -114.21$ and $a_1 = 1.06$. Furthermore, the Δ nvPM EI_n scales proportional to the thrust setting \hat{F} , which is valid for $10\% < \hat{F} < 100\%$. Since nvPM emissions at cruise altitudes contribute to contrail formation, ¹⁰ the thrust setting for cruise, which is typically between 45% and 70% is used to assess the fuel influence. For cruise conditions, Brem et al. ⁵⁸ report $\hat{F} = 65\%$, whereas the supplemental tables from Teoh et al. ¹⁰ list $\hat{F} = 47.5\%$. With the values in Table 2 from Teoh et al., ¹⁰ which

Table 2. Reference Soot Emission Indices

refs	nvPM EI _n [10 ¹⁵ #(kg fuel)]	fuel	H_f	comment
1013	[10 "(kg luci)]	1401	11 j	comment
Märkl et al. ⁹	1	Jet A-1	14.08	global fleet average of all flights from 2019 to 2021
	0.4	HEFA	15.11	
Teoh et al. ¹⁰	0.94	Jet A-1	13.80	flights in the North Atlantic in 2019
	0.46	SAF	15.30	
Teoh et al., ¹⁰ adj.	1.225		13.2604	adjusted to match eq
Barrett et al. ⁶⁴	0.2 [0.01 to 0.6]	not discl	osed	below 3000 ft
	0.4 [0.1 to 6]			above 3000 ft

represent the fleet aggregated emissions in the North Atlantic for 2019, $\hat{F}=54.74\%$ was derived, which is used in this study. Teoh et al. 10 also report absolute measured nvPM, which are utilized to calculate the absolute nvPM from the reference value and eq 8

$$nvPMEI_n = nvPMEI_n(H_{f,ref}, \hat{F}) \cdot \left(1 + \frac{\Delta nvPMEI_n\%}{100.0}\right)$$
(9)

Equation 8 has the benefit of directly relating the influence of the fuel to the particle emissions. However, it does only take into account one property of the fuel, namely, its hydrogen mass content H_f . Therefore, it cannot represent the complex compositions and structures of the components that make up the fuel. These uncertainties are estimated using the experimental data provided by Teoh et al. Globally, the 5th and 95th percentiles correspond to Δ nvPM $EI_{n-10.45}$. However, the errors grow with decreasing Δ nvPM EI_n (or increasing H_f). Therefore, a linear fit was performed for the lower and upper errors depending on the predicted Δ nvPM EI_n . For the fifth percentile, this resulted in $PI_{lower} = (0.161 \cdot \Delta$ nvPM $EI_n) - 1.274$, and $PI_{upper} = (-0.187 \cdot \Delta$ nvPM $EI_n) + 3.172$ for the 95th percentile.

3.2.2.2. Yield Sooting Index. As the correlation for nvPM EI, in the previous section is limited to only one fueldependent parameter being the hydrogen mass content of the fuel (H_t) , a second modeling approach is investigated based on the yield sooting index. The YSI measurement involves doping a fuel into a methane/air flame in a laboratory setting and then analyzing the soot volume fraction that is produced. Doping ensures identical reactive environments, minimizing the effects of flame conditions and temperature variations and isolating the fuel's inherent effect on soot formation.⁵⁹ The data set of more than 400 pure compounds⁶⁰ and also a small number of diesel and jet fuels⁵⁵ enabled the training of the mean matrix model described in Section 3.1.2, which incorporates a more detailed representation of the fuel. However, it lacks a mapping to the actual nvPM emitted, which is the basis for estimating the climate impact, according to Table 1. As the mass-based yield sooting index (YSI_m), where the flame is doped with a constant mass fraction Y_p correlates better with sooting tendencies, 61 it is used instead of its molar counterpart YSI_n to infer the climate impact. The conversion from the mol to mass basis was conducted using the data provided in Das et al.55

$$YSI_{m} = 111.5 \frac{YSI_{n}}{M_{cr}} - 32.3 \tag{10}$$

with $R^2 = 0.99$.

3.2.2.3. Contrail-Induced Cloudiness from Particle Emissions. Burkhardt et al. 11 correlated the radiative forcing with the ice particle number, which is dependent on the exhaust particles. Märkl et al. 19 states that "in the soot-rich regime for temperatures several degrees below the Schmidt-Appleman contrail formation temperature, the decrease in ice crystal numbers is equal to the decrease in emitted soot numbers". This is also affirmed by Teoh et al. 10 (Table 2), where a 51.5% decrease in nvPM EI_n results in a 55.1% decrease in lifetimemean ice particle number per contrail length. Therefore, the nvPM can be correlated to the ice crystal number and thus to the contrail formation and its radiative forcing. Leipold et al. 62 provided a fitting function for the values given in Burkhardt et

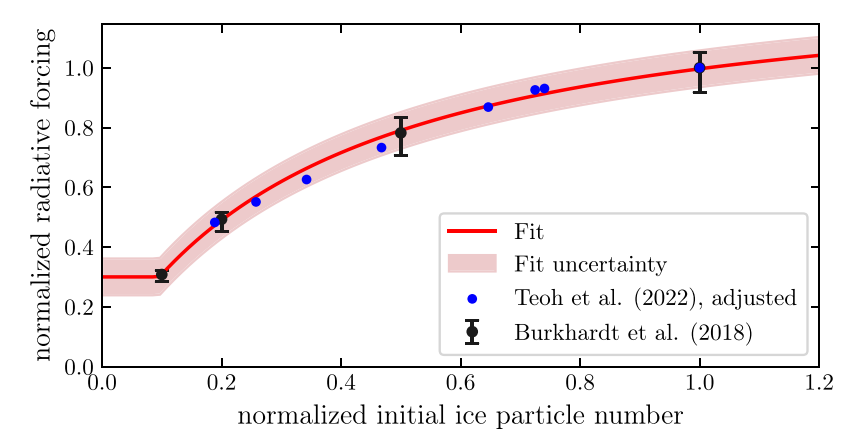


Figure 5. Relative change in radiative forcing (RF) from contrail-induced cloudiness (CiC) on the relative change in ice particle numbers. Data are from Burkhardt et al., 11 fit is based on eqs 11–13, RF reduction is capped at 70%. Data from Teoh et al. 10 as reference, adjusted to match the fit.

al. 11 during the German Aerospace Center (DLR) Development Pathways for Aviation up to 2050 (DEPA 2050) project

$$\widehat{RF} = a \cdot \arctan(b \cdot \widehat{N_{ice}}^c)$$
 (11)

with a=0.92, b=1.9, and c=0.74, where \widehat{N}_{ice} is defined as the ice particle number normalized by the "present-day scenario", and, as outlined earlier, directly correlated to the nvPM EI_n. However, eq 11 is "only valid for [particle matter] reductions less than 90% (i.e., PM of 0.1). As for larger reductions the ambient aerosols become important, the radiative forcing is reduced by a maximum of 70%". Thus, the reduction of the normalized contrail \widehat{RF} is capped at a reduction of $\Delta nvPM$ EI_n = 90% to the baseline soot.

The original data provided in Burkhardt et al. ¹¹ includes uncertainties, which is why a new fit is carried out to incorporate the uncertainties. This leads to the optimal fit parameters

$$X_{\text{opt}} = (a \ b \ c)^{\text{T}}$$

= $(0.87970622 \ 2.13458136 \ 0.7656411)^{\text{T}}$ (12)

and the covariance matrix

$$Cov(X) = \begin{pmatrix} 0.00162589 & -0.00957672 & -0.00115627 \\ -0.00957672 & 0.05895327 & 0.00740328 \\ -0.00115627 & 0.00740328 & 0.00098079 \end{pmatrix}$$
(13

From eqs 12 and 13, the uncertainties of the fit are propagated to the ERF calculations by assuming a multivariate normal distribution $\mathcal{N}(X_{\text{opt}}, \text{Cov}(X))$. The resulting fit and its uncertainties are depicted in Figure 5.

To compare the \widehat{RF} of different fuels, it is essential to know the nvPM EI_n against which the relative reduction is calculated. Burkhardt et al. 11 mention a "present-day scenario" with N_{ice} from $4.5 \cdot 10^{14}$ to $5.5 \cdot 10^{14}$, which is derived from Schumann and Heymsfield, 63 but no absolute values for soot are given. Therefore, a literature review was conducted to find the range of reference soot, which is then used to calculate contrail reduction. Table 2 lists the nvPM EI_n given in different publications. It illustrates that the nvPM EI_n , which can serve as a reference, highly depends on the fuel that is assumed, on the study domain that is considered, and on the flight altitude. Märkl et al. 9 and Teoh et al. 10 report similar values, even

though the reduction for SAF with higher H_f is lower in the latter study. The reference soot EI in Lee et al.³¹ is estimated by Barrett et al.⁶⁴ for conditions below 3000 ft. They also report values above 3000 ft, providing a more realistic picture of typical cruising altitudes (\approx 30,000 ft) and closer agreement with the other studies. With respect to the study domain, Märkl et al.⁹ use the global fleet average for all flights from 2019 to 2021, while Teoh et al.¹⁰ use the average for all flights in the North Atlantic in 2019.

Furthermore, a decrease in contrail RF of 44.8% is reported in Teoh et al. 10 (from jet A-1 with $H_f = 13.8\%$ compared to a SAF with $H_f = 15.3\%$), which originates from a decrease in nvPM EI_n of 51.5% and a decrease in N_{ice} of 55.1%. Equation 11 yields only a reduction in RF of 25% for those values, caused by the different baseline ice particle numbers of the two studies. In this study, an adjusted value of nvPM $EI_n = 1.225$ · 10¹⁵ #/(kg fuel) is used, which fits best with the CiC correlation in eq 11 (cf. Figure 5) and eq 9. Adjusting the baseline soot corresponds to a particle number of $N_{\rm ice} = 4.1$ 10^{12} 1/kg, and a baseline H_f = 13.2604 mass %. In addition to the nvPM EI,, YSI, is used as a competing approach to determine the CiC. However, there is neither a reference YSI,, nor a detailed composition of a fuel representing the fleet average available. Therefore, the NJFCP A-2 POSF10325, "nominal case" (A-2) is used to calculate $YSI_{m,ref=70.3}$.

3.2.2.4. CO_2 and H_2O . The reaction equation for the complete combustion of a hydrocarbon (eq 3) can be used to calculate the EI_m of CO_2 and H_2O from the given H_f (= Y_H), which is taken either directly from an available measurement or from the detailed composition (GCxGC). To determine the EI_m , the amount of substance (n_α) of $m_f = 1$ kg is multiplied by the molar weight and the stoichiometric coefficients given in eq 3, which results in $m_{CO_2} = n_C \cdot M_{CO_2}$ and $m_{H_2O} = n_H/2 \cdot M_{H_2O}$, where $M_{CO_2} = 44$ g/mol, $M_{H_2O} = 18$ g/mol, and the n_α for all $\alpha \in \{C,H\}$ are calculated via

$$n_{\alpha} = \frac{m_f Y_{\alpha}}{M_{\alpha}} \cdot 1000 \frac{g}{\text{kg}} \tag{14}$$

For 1 kg of a typical JET A with $Y_{\rm H} \approx 13.75\%$ this leads to the gaseous emissions of $m_{\rm CO_2} = 3158$ g and $m_{\rm H_2O} = 1234$ g.

3.2.3. Climate Impact. As described in Section 2.3, the climate impact of the individual emissions depends not only on their EI, but also on their respective ERF (cf. Table 1). To assess the climate impact when using a certain fuel, the

different emissions have to be weighted and the total ERF is given by

$$ERF_{tot} = \sum_{i} \left(\frac{EI_{i}}{EI_{i}^{ref}} \right) \cdot ERF_{i}, i \in \{CO_{2}, H_{2}O, NO_{x}, soot$$

$$, contrail cirrus, SO_{x} \}$$
(15)

The respective reference EI^{ref} of the individual emissions is determined as follows. Lee et al. 65 report the reference values listed in Table 1, which represent the average emission indices for the year 2018. These values are the base for the ERFs from Table 1, and result in an $ERF_{tot}^{ref} = 104.74$. For CO_2 , H_2O , and SO_x , the weighting is straightforward, as their direct EIs are known. For NO_x , the EI is heavily dependent on the combustor design and operating conditions and less on the fuel. 44 Therefore, a constant NO_x EI is assumed when comparing different fuels. For soot, and thus also contrail cirrus, the EI^{ref} are discussed in Section 3.2.2.

3.2.4. Correlations for LBO. 3.2.4.1. Lefebvre. According to Lefebvre, 66 $q_{\rm LBO}$, which is the fuel-air ratio (FAR), at which LBO occurs, is

$$q_{\rm LBO} = \left(\frac{A'f_{pz}}{V_c}\right) \left(\frac{\dot{m}_A}{p_3^{1.3} \exp(T_3/300)}\right) \left(\frac{D_0^2}{\lambda_{\rm eff} LCV}\right)$$
(16)

where f_{pz} is the fraction of total combustor air employed in primary-zone combustion, V_c is the total combustion zone volume, \dot{m}_A is the Air mass flow, p_3 and T_3 are the combustor inlet pressure and temperature, respectively, D_0 is the initial mean drop size of the fuel spray, $\lambda_{\rm eff}$ is the effective evaporation rate, and LCV is the lower calorific value of the fuel. The first term on the right side embodies the dependency on the combustor design, the second term represents the operational conditions, and the last term is a function of fuel-dependent properties.

Since the first two terms of eq 16 are independent of the fuel and this study focuses on the fuel influence, the equation can be further simplified to

$$q_{\rm LBO} \propto \frac{D_0^2}{\lambda_{\rm eff} {\rm LCV}}$$
 (17)

The initial diameter D_0 is calculated using a correlation for a prefilming airblast atomizer proposed by El-Shanawany and Lefebyre⁶⁷

$$D_{32} = \left[0.33 We^{0.6} \left(\frac{\rho l}{\rho g} \right)^{0.1} + 0.068 Oh \left[1 + \frac{\dot{m}_l}{\dot{m}_g} \right] d_h \right]$$
(18)

The mass flow ratio of $\dot{m}_g/\dot{m}_l=4.3$, the gas velocity $\mu_g=100$ m/s, the hydraulic diameter $d_h=19.05$ mm, and the characteristic length (which in this case equals the diameter of the prefilmer d_p) $l_c=4.2$ mm were taken from a J79–17A combustor. The Weber number and Ohnesorge number are given by

$$We_{l_c} = \frac{\rho_g \mu_g^2 l_c}{\sigma_l} \tag{19}$$

and

$$Oh_{l_c} = \frac{\mu_l}{\sqrt{\rho_l \sigma_l l_c}} \tag{20}$$

using the liquid properties of the fuel $(\mu_b \ \rho_b \ \sigma_l)$ calculated by the MQSPR model at a temperature of 15 °C.

The effective evaporation rate $\lambda_{\rm eff}$ is calculated using the inhouse Lagrangian particle tracking code SPRAYSIM. The evaporation of single- and multicomponent fuels has been validated for combustion-relevant conditions, with a relative error of about 5%. For $\lambda_{\rm eff}$ an initial droplet temperature of 15 °C is assumed. The droplet with the initial diameter of D_0 (eq 18) is then entered into a domain with $T_g=1300$ K. When the droplet is completely evaporated, the evaporation time $\tau_{\rm evap}$ is used to calculate

$$\lambda_{\text{eff}} = \frac{D_0^2}{\tau_{\text{evap}}} \tag{21}$$

3.2.4.2. Bell. Bell et al. ⁷¹ took a different approach, analyzing experimental LBO data collected during the National Jet Fuels Combustion Program (NJFCP). The combustor rig, which is a swirl-stabilized rich-burn quick-quench lean-burn (RQL) geometry with effusion cooling, ⁷² was developed to specifically act as a referee rig to investigate fuel-sensitive effects in an aircraft main engine. The initial measurements show a strong correlation of LBO with DCN, although fuels that significantly differ from conventional jet fuels are found to have a weaker correlation.

The main impact of the deviation was found to be the preferential vaporization of the droplets that are injected into the combustor. Other studies 73,74 also show an effect of preferential vaporization on both ignition and extinction. Since the lighter, more volatile species in the fuel will evaporate more rapidly than the heavier components, the local vapor fractions can differ from the initial composition of the fuel. Thus, the DCN of the evaporated fraction changes during different stages of evaporation.

Bell et al.⁷¹ computed the DCN throughout the evaporation process and performed a power law regression analysis to identify the best correlation. The best correlation was found to be the DCN of the composition after 34% of the initial volume has evaporated

$$DCN_{34} = DCN(V_{dist} = 0.34V)_g$$
 (22)

However, it is worth noting that this value might change for different combustors. The correlation for $\phi_{\rm LBO}$ follows

$$\frac{\phi_{\text{LBO}_f}}{\phi_{\text{LBO}_{A-2}}} = \left(\frac{\text{DCN}_{34_f}}{\text{DCN}_{34_{A-2}}}\right)^{-0.069}$$
(23)

where the suffix A-2 denotes the DCN and $\phi_{\rm LBO}$ of the A-2 fuel from the NJFCP.

The DCN₃₄ is determined by first calculating the distillation cuts of the fuel that correspond to an evaporated volume of 34%. The composition of the upper cut is then taken as an input for the MQSPR model for the DCN. The distillation cut calculation is based on averaging and sampling the boiling points of the fuels' hydrocarbon composition. However, it is noteworthy that this is an approximation which does not reflect an industrial distillation column or the distillation according to the ASTM D86,⁷⁵ since both processes are not necessarily in thermal equilibrium and distillate the fuel slowly instead of "boiling" it.

3.3. Nondeterministic Approach and Error Propagation. A major aspect in assisting the certification process is the accuracy of the models that predict the properties.¹³ To enable

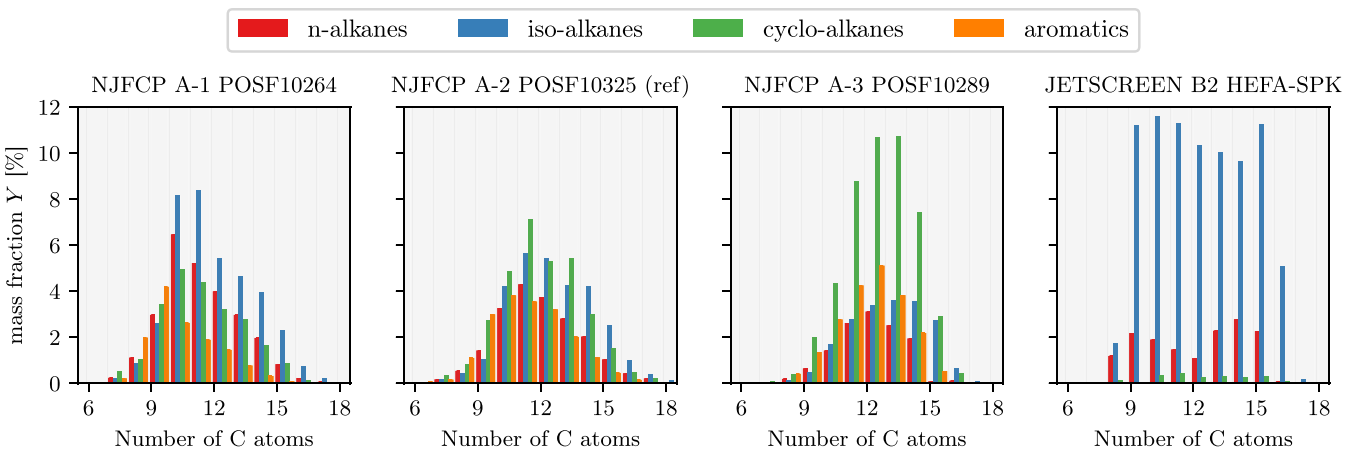


Figure 6. Composition of neat fuels investigated in this study.

Table 3. Measurements and Predictions of Selected Properties for the Neat Fuels Investigated in This Study

	A-1		A-2		A-3		B2	
	exp.	pred.	exp.	pred.	exp.	pred.	exp.	pred.
formula ^a	$C_{10.8}H_{21.8}$		$C_{11.4}H_{22.1}$		C _{11.9} H _{22.5}		$C_{11.6}H_{25.2}$	
$H_{\rm f}^{a}$	14.43		14.01		13.68		15.38	
$T_{10}^{b,e}$	164	$166.7^{+\ 8.9}_{-8.9}$	176	$179.6^{+\ 9.6}_{-9.6}$	198	$193.9^{+10.4}_{-10.4}$	165	158 + 8.5
$T_{50}^{\ \ b,e}$	189	$184.9^{+\ 6.4}_{-6.4}$	205	$196.1^{+\ 6.8}_{-6.8}$	219	$212.5^{+\ 7.4}_{-7.4}$	202	$192^{+\ 6.7}_{-6.7}$
$T_{90}^{\ b,e}$	234	$228.2^{+10.1}_{-10.1}$	244	$240.1^{+10.6}_{-10.6}$	245	$238.1_{-10.5}^{+10.5}$	249	$226^{+10.0}_{-10.0}$
$T_{50} - T_{10}^{\ c}$	25	$18.2^{+15.4}_{-15.4}$	29	$16.5^{+16.4}_{-16.4}$	21	$18.6^{+17.8}_{-17.8}$	37	$34^{+15.2}_{-15.2}$
$T_{90} - T_{10}^{\ c}$	70	$61.5^{+19.0}_{-19.0}$	68	$60.5^{+20.2}_{-20.2}$	47	$44.2^{+20.9}_{-20.9}$	84	68+18.5
$YSI_m^{d,e}$	49.6	$53.0^{+21.6}_{-21.4}$	70.3	$69.8^{+28.7}_{-28.7}$	86.9	$77.9^{+37.4}_{-37.8}$		$21.9^{+13.9}_{-13.9}$
ρ(15 °C) ^{b,f}	780	$783.1^{+\ 6.4}_{-7.7}$	803	$799.2^{+\ 6.8}_{-6.5}$	827	$820.6^{+\ 5.7}_{-8.4}$	752	$752.8^{+10.7}_{-4.4}$
LCV ^{b,f}	43.2	$43.4^{+0.10}_{-0.16}$	43.06	$43.34^{+0.09}_{-0.09}$	42.88	$42.9^{+0.07}_{-0.06}$	44.18	$44.1^{+0.06}_{-0.19}$

^aCalculated from GCxGC. ^bExperimental data from Edwards⁷⁹ for A-1,A-2,A-3, and JETSCREEN⁸⁰ for B2. ^ccalculated from T_{10} , T_{50} , T_{90} dExperimental data from Das et al.⁵⁵ ^ePredictions with mean matrix model. ^fPredictions with MQSPR model.

risk-informed decisions, all known uncertainties must be propagated throughout the models. This also makes it possible to assess whether the difference between the fuels can be accurately resolved. ⁷⁶

In this study, the uncertainties are propagated by using a sampling approach. For each property calculated with the MQSPR approach, an array of samples is returned that takes into account both the isomeric variance and the modeling error inherent in the Gaussian kernel-based model. For the mean matrix, a mean, lower PI, and upper PI are computed from the matrices (Figure 4). From these three values, assuming a split normal distribution, N random samples are drawn that serve as an array input to the empirical models. The split normal distribution, also known as the two-piece normal distribution, joins two halves of a normal distribution at the mode. Due to the different variances of the halves, asymmetric PIs can be considered.

4. FUEL SELECTION—STUDY SETUP

In 2006, the CRC conducted a fuel survey. They obtained a total of 57 jet fuel samples from 18 countries and included JET A, A-1, JP-5, and JP-8 fuels. The study results revealed a significant variability in composition and thus properties. Reflecting the spectrum of available jet fuels, the metrics of these fuels serve as a baseline reference data set for comparison. The reference data set includes measured values for the density at 15 °C, distillation slopes ($T_{90} - T_{10}$ and $T_{50} - T_{10}$), kinematic viscosity at -40 °C, specific energy (LCV),

and aromatic content. All other metrics are predicted from the respective fuel compositions. Furthermore, three representative fuels were selected from within this spectrum, building on the prior identification by the NJFCP:⁷⁷ One JP-8 fuel with a low flammability limit, low viscosity, and low aromatic content (A-1), one JET-A fuel with properties very close to the CRC average properties (A-2) and one JP-5 fuel with high flammability, viscosity, and aromatic content (A-3). These properties were originally "selected by the original equipment manufacturers (OEMs)⁷⁸ as a best-performing, averageperforming, and worst-performing jet fuel with respect to the performance of the critical metrics". To this study, all properties of the three conventional fuels are predicted values. Figure 6 shows the composition of the unblended fuels. The three conventional fuels vary in their composition, A-1 having higher n- and iso-alkanes, whereas A-3 contains more cycloalkanes and aromatics. The A-2 is situated between the other

The variation in compositions leads to the variation in the selected properties shown in Table 3. The table validates the Mean Matrix model for the distillation and the YSI_m for the investigated fuels. It is noteworthy that the PIs are significant for both properties due to the high variance in boiling points and YSI_m for the different isomers for each fuel family and carbon number. Nevertheless, the YSI_m predictions for the NJFCP fuels are close to the measured values and correctly represent the trend between the fuels. For the distillation, all measurements are within the prediction intervals except T_{50} of

A-2 and JETSCREEN B2 HEFA-SPK (B2) and T_{90} of B2. Nonetheless, all distillation slopes are within the PIs. Therefore, the Mean Matrix model is capable of predicting the distillation slopes and YSI_m. For the other metrics, the implementation was verified with the data from the literature they originate: payload and range, ²⁹ nvPM EI_m, ¹⁰ and ERF. ⁶⁵

For the performance and emissions metrics, as well as for the LBO, no specification limits are set by the ASTM. ^{3,22} Thus, the CRC data set is used to evaluate whether a SAF is within the range of experience of already approved jet fuels. For the assessment of the performance of SAF, A-2 fuel is chosen as the reference from which the improvements or deterioration of SBCs and blends thereof will be calculated. The other two fuels (A-1, A-3) cover a substantial portion of the CRC data set range. Regarding density, A-1 and A-3 fuels even fall outside the CRC data range. This qualifies the two fuels to be used in the blending study to explore the limits of blending ratios before a mixture exceeds the specification limits.

Among the various SBC production pathways, standardized and qualified in ASTM D7566,3 HEFA-SPK is currently the most widely available option. The fuel produced from hydroprocessed esters and fatty acids relies on refined oil from biomaterial such as crop plants (e.g., rapeseed or soy), animal fat, or used cooking oils. It accounts for 80% of the current SBC production and is a key enabler to ramp up SAF production for reaching net zero carbon emission by 2050.81 It is currently certified to be blended with conventional jet fuel up to a volume fraction of 50%.³ Thus, HEFA-SPK is selected as the SBC candidate for the blending study, more precisely B2 being representative of the average properties of HEFA-SPKs, as reflected in the DLR SimFuel-database. It was thoroughly investigated during the JET Fuel SCREENing and Optimization (JETSCREEN) program. Its composition differs from the conventional jet fuels (Figure 6), with most of it being isoalkanes, followed by n-alkanes and a small fraction of cycloalkanes. Due to the absence of aromatics, it makes the HEFA-SPK a candidate to reduce emissions but also leads to a lower density, which will restrict its blending potential under the current ASTM specifications. To examine the feasibility of the ReFuelEU blending mandate (Figure 1) and the potential added values, HEFA-SPK is blended with A-1 and A-3 from 10 to 70%.

5. RESULTS AND DISCUSSION

5.1. Conventional Fuels. The metrics introduced in this study are first evaluated using the three conventional fuels A-1, A-2, and A-3.

5.1.1. Performance. First, the performance metrics and the structure of the plots will be discussed. Figure 7 shows the metrics regarding range and fuel uptake as well as the main contributors to these metrics, the gravimetric energy density (specific energy, LCV, e) and volumetric energy density (U). The plot is structured in a way that keeps the reference fuel (A-2) in the center and only shows the percentage deviation of the other fuels to it. The colored regions around each line indicate the prediction intervals (PIs) of each property. The bar and whisker plots below each axis show the range of the CRC data set.

First of all, it is noticeable that the A-1 and A-3 fuels are near the edges of the CRC range, as intended. In addition, A-2 is situated in between, near, or inside the interquartile range of the CRC fuels. Looking at the volumetric energy density and gravimetric energy density, the two metrics appear to have an

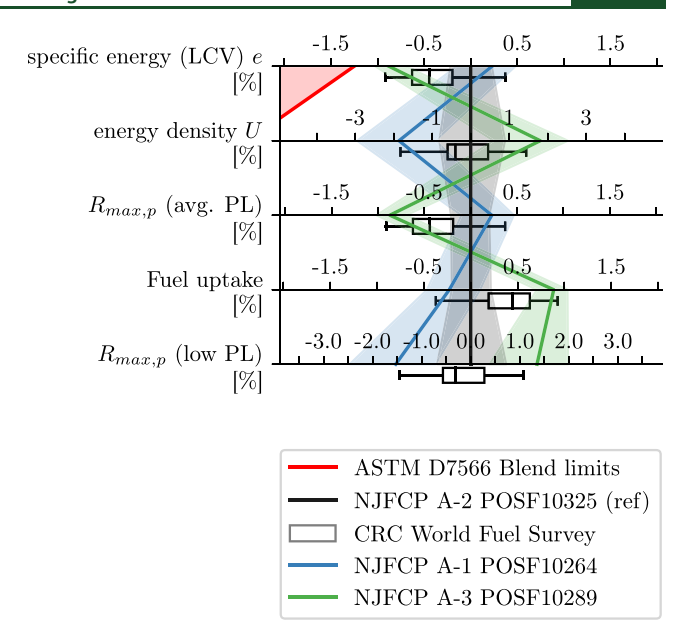


Figure 7. Performance metrics for the three reference fuels. The *x*-axis depicts the relative deviation from the A-2 fuel. Colored areas represent the PIs, and red areas represent the specification limits.

inverse relationship. While the A-1 has a high e due to its high LCV, it has a lower volumetric energy density due to its lower density, which is caused by its high content of n- and iso-alkanes compared to the other two fuels. The opposite is true for the A-3 fuel. This behavior underlines the necessity to look at different flight missions.

The $R_{\rm max,p}$ for average payload, is improved for A-1. For this flight mission, only the gravimetric energy density (LCV) has an impact since the range is only influenced by W_0 and not the volume of the fuel tank. The same applies for the fuel uptake, where the plane fueled by A-1 can fly the selected route with less fuel. In this specific scenario, the range and fuel uptake are directly proportional to the gravimetric energy density of the fuel, which is highest for n- and iso-alkanes and lower for cyclo-alkanes and aromatics. Shape The $R_{max,p}$ for low payload, however, shows a different behavior. Since this flight mission is limited by the fuel volume, a higher volumetric energy density and thus density are preferable to fit a maximum amount of energy into the available volume.

The densities, which are listed in Table 3, reflect the same trend. The A-3 outperforms the other fuels due to its high content of *cyclo*-alkanes and aromatics and the higher amount of components with higher carbon numbers.

5.1.2. Emissions. The evaluation of emission metrics (Figure 8) begins with an examination of the individual EIs. Regarding soot, both the empirical correlation by Teoh et al. (eq 8) and the YSI_m yield similar results, even though the axes are scaled differently due to the larger PIs of the YSI_m model. In both cases, A-1 produces roughly 20% less soot than A-2 due to its lower H_f which is caused by the lower content in *cyclo*-alkanes and aromatics. Indicating how "clean" the neat A-1 fuel is, it even is well outside the CRC range, except for one CRC fuel. This outlier is a 50% blend of Sasol's FSJF (CRC sample number 507). It is also worth mentioning that the uncertainties in the soot predictions (both nvPM EI_n and YSI_m) are comparatively high, so that the difference between fuels that are close to each other can not accurately be resolved.

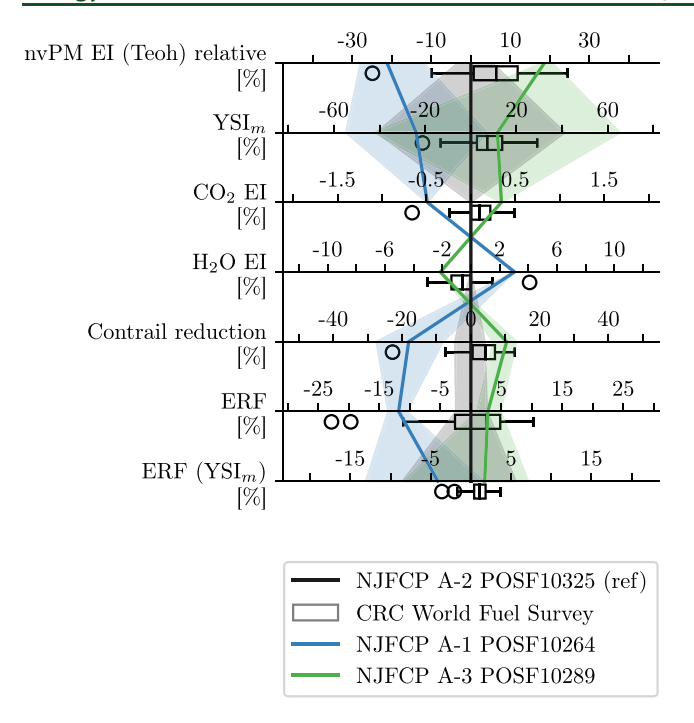


Figure 8. Emission metrics for the three reference fuels. The *x*-axis depicts the relative deviation from the A-2 fuel. Colored areas represent the PIs. The PIs for ERF only include input and modeling uncertainties but not the uncertainties from Table 1 due to their large magnitude.

The gaseous emissions CO_2 and H_2O show similar trends due to their dependence on H_{f_1} even though their overall differences are smaller than for the soot. The outlier in the CRC data again stands out. The CO_2 emissions are directly proportional to Y_C , and the H_2O emissions are proportional to Y_H . Thus, with $Y_C + Y_H = 1$, they are negatively proportional. However, according to Table 1, the ERF and thus climate impact of CO_2 by far exceeds the one of H_2O . As a consequence, minimizing CO_2 emissions should take precedence over reducing H_2O .

The reduction in CiC follows the same pattern as the soot metrics, as the nvPM EI_n (and thus H_f) is the only parameter in that correlation. However, due to the nonlinearity in eq 11, the decrease in CiC is larger for A-1 compared to A-2 than for A-2 compared to A-3, even though the differences in nvPM EI_n are similar. This is also reflected in the reduction of overall radiative forcing using nvPM EI_n as an input. The ERF based on YSI_m shows smaller differences between the fuels. That again can be explained by the different baseline soot emissions that are used. As the PIs of the ERF account for input uncertainties, the resulting YSI_m-based ERF exhibits greater uncertainty than the distinctions between the fuels.

5.1.3. Safety. Addressing the safety metrics for the three reference fuels, Figure 9 is split into two parts. The LBO metrics are plotted in the same way as the performance and emission metrics, with the A-2 fuel in the center and the percent deviations on the x-axis. The other properties, which correspond to a selected set of specifications for the final blend, defined in ASTM D7566 Table 1, are plotted with their absolute values, and the specification limits are depicted in red. As a result, stakeholders can easily recognize the established limits.

Starting with the LBO metrics, several things stand out. First, the uncertainties for both correlations are large. The

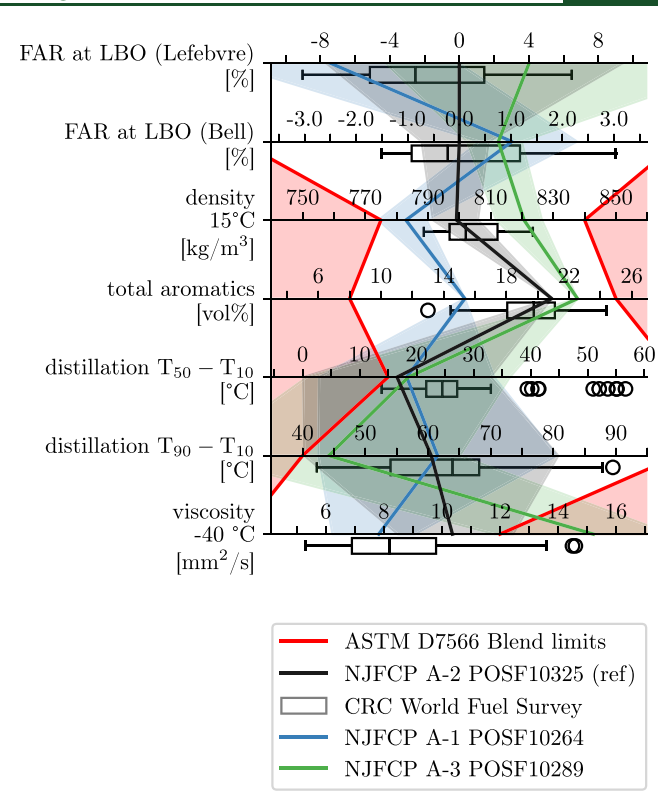


Figure 9. Safety metrics for the three reference fuels. The *x*-axis depicts the relative deviation from the A-2 fuel for LBO. Properties that have limits according to ASTM D7566³ are plotted as absolute values. Colored areas represent the PIs, red areas the specification limits.

main contributor to the PIs is the kinematic viscosity ν , which is difficult to predict at the given temperatures (15 °C), since the majority of the data to train the model is available at -20 °C. Second, the ranking of the fuel changes depending on the used correlation. The two correlations even contradict each other. A possible explanation for this discrepancy is the variation in the combustor types and selected operating conditions used to develop the correlations. An additional factor contributing to uncertainty is the specific methodology used by the Bell correlation to determine the distillation cut used for the DCN prediction. Thus, no clear decision can be made on which fuel is better in terms of the LBO behavior. However, the range of CRC fuels can still be used to identify if a fuel exhibits anomalous LBO behavior.

The ranking between the LBO for the Lefebvre and McDonell correlation (eq 16) can be explained by the fuel compositions. ⁸² In general, a lower LCV, as well as a higher ν and ρ (leading to a higher D_0), together with a longer $\tau_{\rm evap}$ (and thus lower $\lambda_{\rm eff}$) lead to a higher (i.e., worse) $q_{\rm LBO}$. All of this applies to A-3 fuel: The LCV is lower due to its high aromatics content, ν and ρ are higher due to its high content in *cyclo*-alkanes, aromatics, and longer chain length (C_{11.9} compared to C_{10.8} for A-1 and C_{11.4} for A-2), while the latter also leads to a higher $\tau_{\rm evap}$.

Looking at the specification limits, it is again obvious that the selected fuels are within the CRC range. However, as already pointed out, ²³ some of the CRC fuels are close $(T_{50} - T_{10}, T_{90} - T_{10})$ or even outside (kinematic viscosity at -40 °C) the ASTM D7566 blend limits. The latter is also true for A-3 fuel. Despite that, all of those are approved jet fuels under

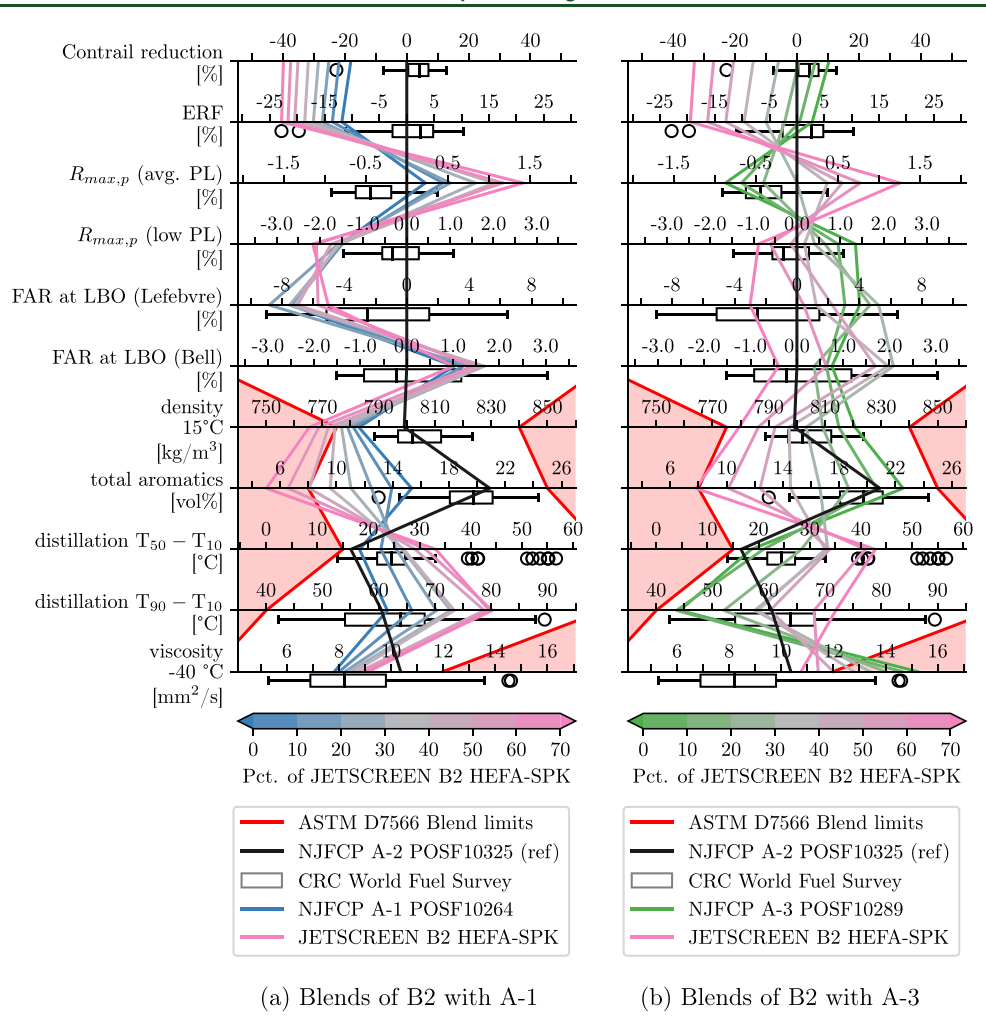


Figure 10. Selected metrics for blends of B2 with A-1 (left) and A-3 (right).

ASTM D1655, because the three properties are not part of the limits for conventional jet fuels.

The distillation slopes, which describe how fast or slow a fuel evaporates, exhibit large uncertainties. One reason, just as for the LBO (Bell), is due to the uncertainties of the distillation model itself (see Table 3). The second reason is the method to determine their PIs: It ranges from the largest difference between the two distillation temperatures $PI_{upper} = (T_{50} +$ $PI_{T_{50}upper}$) – $(T_{10} - PI_{T_{10}lower})$ to the smallest difference PI_{lower} = $(T_{50} - PI_{T_{50}lower}) - (T_{10} + PI_{T_{10}upper})$. That way, the PIs of the distillation slopes exceed the PIs of the single distillation temperatures (T_{10}, T_{50}, T_{90}) . Despite this, it is worth mentioning that all three conventional fuels have a low T_{50} - T_{10} , whereas only A-3 is close to the limits for T_{90} - T_{10} . The uncertainties in the viscosity predictions are large as well, as already mentioned for the LBO (Lefebvre), where the viscosity made a significant contribution to its uncertainty. Nevertheless, even considering that the A-3 might lie at the lower end of its prediction interval, it would still be outside the ASTM D7566 blend limits.

5.2. HEFA-SPK Blends. The previous section showed the bandwidth of conventional jet fuels and that the selected fuels (A-1 and A-3) are a good baseline to evaluate the added values of blending SBCs. As mentioned at the beginning of this section, a HEFA-SPK fuel is selected for a blending study. The blending of the fuels is carried out using their respective

detailed compositions, as measured by GCxGC analysis. The blend composition is then defined as $\Xi_{\text{blend}} = \sum_k (w_k \Xi_{i,j_k})$, where the index k denotes the different components of the blend, i is the carbon number, j is the fuel family, and w_k is the volume fraction of each blend component. The resulting Ξ_{blend} is then used as an input to the models predicting the metrics.

In contrast to the previous section, all metrics are shown collectively in one plot (Figure 10) while some metrics are left out, since they are included in other metrics (e.g., nvPM EI_n in the ERF). The plot is split into two halves: the left one contains all blends of HEFA-SPK with A-1, the right one all blends of HEFA-SPK with A-3. The different blends are color-coded according to their blend ratio.

Starting with the emissions, all blends lead to a significant reduction in contrails and also ERF. The 70% HEFA-SPK/A-1 blend leads to a reduction in ERF of around 10 percentage points (pt) compared to neat A-1. For the same blend ratio with A-3, the reduction is even more significant (20 pt). The main contribution to the ERF reduction is the higher H_f of the blends, which reduces both CO_2 and nvPM EI_n , and due to the latter also the CiC.

Furthermore, the blending shows significant improvements in the maximum range for the average payload case, caused by the increased gravimetric energy density. Even with a blend ratio of just 30%, the A-3 fuel performs almost as well as the A-2, and with 40% it exceeds the CRC range. In contrast, due to

the lower density of the HEFA-SPK, the low payload case worsens, which again highlights the necessity to consider different use cases.

Just as for the conventional fuels, the LBO correlations show some anomalies. The Lefebvre model predicts a worse (higher) FAR for the HEFA-SPK/A-1 blend compared to neat A-1, but a significant improvement when blended with A-3. However, the trends do not monotonously increase or decrease with changing blend ratios. This suggests that the model is not capable of properly handling fuel blends. The most likely culprit for this behavior is the model used to predict λ_{eff} as it models the composition inside each fuel family with probability density functions, which are not capable of handling compositions with multiple peaks. Equally, the model of Bell shows nonmonotonous behavior and suggests that the medium-percentage blends (30 to 50%) behave significantly worse than the others. This is again due to either the distillation cut calculation or the applicability of the correlation to blends, which has not yet been validated. Overall, the study's findings imply that the existing models may oversimplify or not fully capture the complex phenomena of LBO, and a revised model that better captures its complexities is required.

Lastly, the specification limits play a crucial role. It is important to recognize that optimizing fuels for better emissions and performance is worthwhile only if they can meet the necessary specification limits and gain approval for use. For the A-1 blends, it becomes evident that the density and the aromatic content are the limiting factors, allowing a maximum blend ratio of 40% and thus a maximum reduction in ERF of roughly 6 pt compared with neat A-1. For A-3, a different picture unfolds. Due to its high density and aromatic content, these properties are not limiting the blend ratio. The blending even improves the distillation slope, moving it away from the respective limits. On the other hand, there exists a lower blending limit of 50% HEFA-SPK, below which the blend would fall outside of the ASTM D7566 kinematic viscosity limits due to the high viscosity of the A-3.

The overall results showcase the potential and limitations of the model-based assessment of an SBC and its blends. It highlights the importance of considering a broad range of metrics and complementary models to enable confident decision making and identify potential risks. Moreover, it is essential to incorporate a range of conventional fuels when blending studies. It also affirms that efforts to effectively use the limited supply of SBCs and to maximize their potential are crucial. Among others, these are targeted for use on flights with a high likelihood for significant contrail-induced climate warming and blending them with high-sooting conventional fuels. Future work should focus on extending the number of metrics and further enhancing the modeling of current metrics to reduce their uncertainties. This can be accomplished either by using more complex models or by extending the database used for the training of the MQSPR and Mean Matrix model.

6. SUMMARY AND OUTLOOK

This study presents a novel, model-based framework to evaluate the added value of SAF across performance, emissions, and safety metrics. Through the integration of machine-learning-based property predictions and empirical correlations, the framework provides an efficient tool for assessing the environmental and operational impacts of SBCs and their blends with conventional fuels. The study showcases

a selected HEFA-SPK with significant potential for improving aircraft performance through enhanced specific energy, which increases the range of an aircraft. Additionally, the findings indicate that the HEFA-SPK can substantially reduce emissions, particularly nvPM, thereby mitigating contrailinduced radiative forcing.

However, the study also identifies challenges associated with blending high fractions of HEFA-SPK with conventional jet fuels, particularly regarding specific property limits, such as density and aromatics. Moreover, reaching the currently certified blend ratio of 50% HEFA-SPK can be a significant hurdle depending on the specific characteristics of the conventional fuel being used for blending. Furthermore, gaps in the modeling methodology, in particular, for LBO, are identified. The discrepancies observed in LBO predictions highlight the complexity of such fuel-related phenomena, indicating that a more accurate modeling of the subprocesses is essential.

The findings also emphasize the importance of a holistic approach to SAF evaluation, supporting the continued development of fuel-sensitive predictive models that also incorporate a wider range of metrics. Future studies should prioritize the development of a more comprehensive data set for SBCs to enhance the accuracy and reliability of the machine learning models. Additionally, further refinement of the modeling approaches for the critical metrics is necessary to ensure that the predictions are useful for decision making and informing policy. As the aviation industry pursues sustainability, these efforts will be crucial in facilitating the transition toward the adaptation of SAF.

ASSOCIATED CONTENT

Supporting Information

The Supporting Information is available free of charge at https://pubs.acs.org/doi/10.1021/acs.energyfuels.5c03162.

Description of safety-relevant properties, emissions, and calculation procedure for payload and range (PDF)

AUTHOR INFORMATION

Corresponding Author

Stephan Ruoff — German Aerospace Center (DLR), Institute of Combustion Technology, Stuttgart 70569, Germany;
orcid.org/0000-0001-9570-7399; Email: stephan.ruoff@dlr.de

Authors

Georg Eckel — German Aerospace Center (DLR), Institute of Combustion Technology, Stuttgart 70569, Germany

Uwe Bauder — German Aerospace Center (DLR), Institute of Combustion Technology, Stuttgart 70569, Germany;

orcid.org/0000-0002-5019-6043

Patrick Le Clercq — German Aerospace Center (DLR), Institute of Combustion Technology, Stuttgart 70569, Germany; © orcid.org/0000-0001-6011-5625

Manfred Aigner – German Aerospace Center (DLR), Institute of Combustion Technology, Stuttgart 70569, Germany

Complete contact information is available at: https://pubs.acs.org/10.1021/acs.energyfuels.5c03162

Notes

The authors declare no competing financial interest.

ABBREV	TATIONS	$n \ \Omega$	amount of substance
nvPM	nonvolatila particulata matter	22 P	mean occurrence matrix mean property matrix
ASTM	nonvolatile particulate matter American Society for Testing and Materials	p	pressure
CAEP	Committee on Aviation Environmental Protec-	$q_{ m LBO}$	fuel-air ratio at lean blowout
	tion	R	range
CI	confidence interval	Σ	standard deviation matrix
CiC	contrail-induced cloudiness	$R_{\max,p}$	maximum range for given payload
CRC	Coordinating Research Council	SP	specific payload
DCN	derived cetane number	SR	specific range
DEPA 2050	Development Pathways for Aviation up to 2050	T	temperature
DLR	German Aerospace Center	U	volumetric energy density
EASA	European Union Aviation Safety Agency	и	velocity
ECLIF	emission and climate Impact of alternative fuel	V_c	total combustion zone volume
EI	emission index	V	volume
ERF	effective radiative forcing	$W_{f_{R,p}}$	fuel weight for given range and payload
FAR	fuel-air ratio	W_0	takeoff weight
FSJF	fully synthetic jet fuel	W_e	empty weight
GCxGC	2D gas chromatography	W_f	fuel weight maximum weight
GHG	greenhouse gas	$W_{ m max}$	payload weight
H/C	hydrogen-to-carbon ratio	W_p	weighting factor
HEFA	hydroprocessed esters and fatty acids	$egin{array}{c} w_k \ Y \end{array}$	mass fraction
ICAO	International Civil Aviation Organization	YSI_m	mass-based yield sooting index
	JET Fuel SCREENing and Optimization	YSI_n	mole-based yield sooting index
LBO	lean blowout	ρ	density
MQSPR	mean quantitative structure-property relation-	$\phi_{ ext{LBO}}$	equivalence ratio at lean blowout
NHECD	ship	$ ho_{ m eff}$	effective evaporation rate
NJFCP	National Jet Fuels Combustion Program	μ	dynamic viscosity
OEM	original equipment manufacturer	ν	kinematic viscosity
PI	prediction interval	Ψ	property
PL	payload	σ	surface tension
QSPR RF	quantitative structure—property relationship	$ au_{ m evap}$	evaporation time
RFNBO	radiative forcing	Ξ	composition matrix
	renewable fuels of nonbiological origin	α	species α
RQL SAF	rich-burn quick-quench lean-burn sustainable aviation fuel	C	carbon
Sasol	South African Synthetic Oil Limited	С	characteristic
SBC	synthetic blend component	dist	distilled
SN	smoke number	evap	evaporated
SPK	synthetic paraffinic kerosene	f	fuel
TSI	threshold sooting index	g	gas
UQ	uncertainty quantification	H	hydrogen
YSI	yield sooting index	h	hydraulic
c_T	thrust specific fuel consumption	1	liquid
D_0	Initial diameter	mix	mixture
D_{32}	sauter mean diameter	opt	optimal
d	diameter	p	prefilmer
EI_m	mass emission index	ref	reference
EI_n^m	number emission index	tot	total
e "	gravimetric energy density	Oh	Ohnesorge number
\hat{F}	engine thrust setting	We	Weber number
f_{pz}	fraction of total combustor air employed in	\mathcal{N}	multivariate normal distribution
J P2	primary-zone combustion	g	gravity of earth
ΔH	arithmetic difference of H _f		
H_f	hydrogen mass content of the fuel		
LCV	lower calorific value of the fuel	■ REFF	RENCES
L/D	Lift-to-Drag ratio		
1	length	-	pean Parliament FIT FOR 55 PACKAGE UNDE
M	molar weight		AN GREEN DEAL: Legislative Train Schedule vw.europarl.europa.eu/legislative-train/package-fit-fo
.1.	Air mass flory	iiiips.//ww	caropari.caropa.ca/ icgisiative-train/ package-in-ic

ER THE ıle 2024 https://www.europarl.europa.eu/legislative-train/package-fit-for-55.

(2) European Parliament and of the Council of the EU Regulation (EU) 2023/2405 of 18 October 2023 on ensuring a level playing field for sustainable air transport (ReFuelEU Aviation). 2023 http://data. europa.eu/eli/reg/2023/2405/oj.

Air mass flow

mass flow rate

ice particle number

mass

 \dot{m}_A

m

m

 $N_{\rm ice}$

- (3) ASTM D7566. Specification for Aviation Turbine Fuel Containing Synthesized Hydrocarbons, D7566–22a; ASTM2022.
- (4) Biomass Research and Development Board SAF Grand Challenge Roadmap: Flight Plan for Sustainable Aviation Fuel 2022 https://www.energy.gov/sites/default/files/2022-09/beto-saf-gc-roadmap-report-sept-2022.pdf.
- (5) Federal Aviation Administration (FAA). United States Aviation Climate Action Plan 2021 https://www.faa.gov/sites/faa.gov/files/2021-11/Aviation_Climate_Action_Plan.pdf. Accessed: May 26, 2025.
- (6) Voigt, C.; Kleine, J.; Sauer, D.; et al. Cleaner burning aviation fuels can reduce contrail cloudiness. *Commun. Earth Environ.* **2021**, *2*, No. 114.
- (7) Boehm, R. C.; Faulhaber, C.; Behnke, L.; Heyne, J. The effect of theoretical SAF composition on calculated engine and aircraft efficiency. *Fuel* **2024**, *371*, No. 132049.
- (8) Le Clercq, P.; Voigt, C.; Sauer, D.et al. In *Emission and Climate Impact of Alternative Fuels: The ECLIF1 and ECLIF2 Campaigns*, Proceedings of the 9th European Conference for Aerospace Sciences; Lille: France, 2022 DOI: 10.13009/EUCASS2022-7260.
- (9) Märkl, R. S.; Voigt, C.; Sauer, D.; et al. Powering aircraft with 100% sustainable aviation fuel reduces ice crystals in contrails. *Atmos. Chem. Phys.* **2024**, *24*, 3813–3837.
- (10) Teoh, R.; Schumann, U.; Voigt, C.; Schripp, T.; Shapiro, M.; Engberg, Z.; Molloy, J.; Koudis, G.; Stettler, M. E. Targeted use of sustainable aviation fuel to maximize climate benefits. *Environ. Sci. Technol.* **2022**, *56*, 17246–17255.
- (11) Burkhardt, U.; Bock, L.; Bier, A. Mitigating the contrail cirrus climate impact by reducing aircraft soot number emissions. *npj Clim. Atmos. Sci.* **2018**, *1*, No. 37, DOI: 10.1038/s41612-018-0046-4.
- (12) Yang, H.; Guo, S.; Xie, H.; Wen, J.; Wang, J. Evaluation of machine learning models for predicting performance metrics of aeroengine combustors. *Case Studies Therm. Eng.* **2025**, *65*, No. 105627.
- (13) Heyne, J.; Rauch, B.; Le Clercq, P.; Colket, M. Sustainable aviation fuel prescreening tools and procedures. *Fuel* **2021**, 290, No. 120004.
- (14) Kosir, S. T.; Behnke, L.; Heyne, J. S.; Stachler, R. D.; Flora, G.; Zabarnick, S.; George, A.; Landera, A.; Bambha, R.; Denney, R.; Gupta, M. In *Improvement in Jet Aircraft Operation with the Use of High-Performance Drop-in Fuels*; AIAA Scitech 2019 Forum, AIAA, 2019
- (15) Boehm, R. C.; Yang, Z.; Bell, D. C.; Feldhausen, J.; Heyne, J. S. Lower heating value of jet fuel from hydrocarbon class concentration data and thermo-chemical reference data: An uncertainty quantification. *Fuel* **2022**, *311*, No. 122542.
- (16) Yang, Z.; Boehm, R. C.; Bell, D. C.; Heyne, J. S. Maximizing Sustainable aviation fuel usage through optimization of distillation cut points and blending. *Fuel* **2023**, *353*, No. 129136.
- (17) Feldhausen, J. J.; Bell, D. C.; Kosir, S. T.; Heyne, J. S.; Scown, C.; Rapp, V.; Comesana, A. *The Co-Optimization of Sustainable Aviation Fuel: Cost, Emissions, and Performance, AIAA Scitech* 2021 Forum; AIAA: Reston, VA, 2021.
- (18) Hall, C.; Rauch, B.; Bauder, U.; Aigner, M. Comparison of probabilistic jet fuel property models for the fuel screening and design. *Fuel* **2023**, *351*, No. 128965.
- (19) Hall, C.; Creton, B.; Rauch, B.; Bauder, U.; Aigner, M. Probabilistic Mean Quantitative Structure-Property Relationship Modeling of Jet Fuel Properties. *Energy Fuels* **2022**, *36*, 463–479.
- (20) Hall, C.; Rauch, B.; Bauder, U.; Le Clercq, P.; Aigner, M. Predictive Capability Assessment of Probabilistic Machine Learning Models for Density Prediction of Conventional and Synthetic Jet Fuels. *Energy Fuels* **2021**, *35*, 2520–2530.
- (21) Hadaller, O.; Johnson, J. World Fuel Sampling Program 2006.
- (22) ASTM D1655. Standard Specification for Aviation Turbine Fuels, D1655-13; ASTM2009.
- (23) Zschocke, A. High biofuel blends in aviation (HBBA). *Interim Rep ENER C* **2012**, *2*, 420–421.
- (24) US Department of Defense. Aerospace Fuels Certification, U.S. Department of Defense, MIL-HDBK-510A, 2014.

- (25) Edwards, J. T. Jet Fuel Properties; DTIC, 2020.
- (26) Victor, B. The Influence of Fuel Properties on Threshold Combustion in Aviation Gas Turbine Engines, Dissertation; University of Cape Town: Cape Town, 2017.
- (27) Moses, C. A. Jet Fuel "Aromatics Effects" And "Distillation Slope" Research Survey., 2012.
- (28) De Klerk, A. Biofuels for Aviation; Elsevier, 2016; pp 241-259.
- (29) Blakey, S.; Wilson, C. W.; Farmery, M.; Midgley, R. Fuel effects on range versus payload for modern jet aircraft. *J. Aeronaut. Sci.* **2011**, 115, 627–634.
- (30) Bureau of Transportation Statistics Data Bank 28IS T-100 and T-100(f) International Segment Data, U.S. and Foreign Air Carriers Traffic and Capacity Data 2025 https://www.bts.gov/browse-statistical-products-and-data/bts-publications/%E2%80%A2-data-bank-28is-t-100-and-t-100f. Accessed: May 26, 2025.
- (31) Lee, D. S.; Allen, M. R.; Cumpsty, N.; Owen, B.; Shine, K. P.; Skowron, A. Uncertainties in mitigating aviation non-CO 2 emissions for climate and air quality using hydrocarbon fuels. *Environ. Sci.:* Atmos. **2023**, *3*, 1693–1740.
- (32) Jacob, D.; Rindlisbacher, T. The landing and take-off particulate matter standards for aircraft gas turbine engines. *ICAO Environ. Rep.* **2019**, 100–105.
- (33) Penner, J. E.; Lister, D. H.; Griggs, D. J.; Dokken, D. J.; McFarland, M. Prepared in collaboration with the Scientific Assessment Panel to the Montreal Protocol on Substances that Deplete the Ozone Layer. In *Aviation and the Global Atmosphere*; University of Cambridge, 1999; p 373.
- (34) International Civil Aviation Organization (ICAO). Committee on Aviation Environmental Protection (CAEP) Report of the Tenth Meeting (Doc 10069), ICAO2016.
- (35) International Civil Aviation Organization (ICAO). Committee on Aviation Environmental Protection (CAEP) Report of the Eleventh Meeting (Doc 10126), ICAO2019.
- (36) McEnally, C.; Pfefferle, L. Improved sooting tendency measurements for aromatic hydrocarbons and their implications for naphthalene formation pathways. *Combust. Flame* **2007**, *148*, 210–222
- (37) Calcote, H. F.; Manos, D. M. Effect of molecular structure on incipient soot formation. *Combust. Flame* **1983**, *49*, 289–304.
- (38) Boehm, R. C.; Zhibin, Y.; Heyne, J. S. Threshold Sooting Index of Sustainable Aviation Fuel Candidates from Composition Input Alone: Progress toward Uncertainty Quantification. *Energy Fuels* **2022**, *36*, 1916–1928.
- (39) Kärcher, B. Formation and radiative forcing of contrail cirrus. *Nat. Commun.* **2018**, *9*, No. 1824.
- (40) Bier, A.; Burkhardt, U.; Bock, L. Synoptic Control of Contrail Cirrus Life Cycles and Their Modification Due to Reduced Soot Number Emissions. *J. Geophys. Res.: Atmos.* **2017**, *122*, No. 11584.
- (41) Mishra, R. K.; Chandel, S. Soot Formation and Its Effect in an Aero Gas Turbine Combustor. *Int. J. Turbo Jet-Engines* **2019**, *36*, 61–73.
- (42) Patil, A.; Bedke, A. C.; Deshmukh, V. A.; Shevare, P. Y. Engine Performance On Atomization Of Fuel Injector: A Review. *Grad. Res. Eng. Technol.* **2022**, 49–53.
- (43) Qiu, C.; An, S.; Shang, Y.; Chen, S. Research on the effect of cavitation on fuel atomization characteristics by molecular dynamics simulation. *Mod. Phys. Lett. B* **2019**, 33, No. 1950259.
- (44) Harlass, T.; Dischl, R.; Kaufmann, S.; et al. Measurement report: In-flight and ground-based measurements of nitrogen oxide emissions from latest-generation jet engines and 100% sustainable aviation fuel. *Atmos. Chem. Phys.* **2024**, 24, 11807–11822.
- (45) National Institute of Standards and Technology (NIST). Standard Reference Database 103a: NIST ThermoData Engine Version 10.4.5 Pure Compounds. https://www.nist.gov/mml/acmd/trc/thermodata-engine/srd-nist-tde-103a.
- (46) Design Institute for Physical Properties DIPPR 801 Database. https://www.aiche.org/dippr/events-products/801-database.
- (47) Kim, S.; Chen, J.; Cheng, T.; Gindulyte, A.; He, J.; He, S.; Li, Q.; Shoemaker, B. A.; Thiessen, P. A.; Yu, B.; et al. PubChem 2019

- update: improved access to chemical data. *Nucleic Acids Res.* **2019**, 47, D1102—D1109.
- (48) Royal Society of Chemistry. ChemSpider. https://www.chemspider.com/.
- (49) Ajmani, S.; Rogers, S. C.; Barley, M. H.; Livingstone, D. J. Application of QSPR to Mixtures. *J. Chem. Inf. Model.* **2006**, 46, 2043–2055.
- (50) Saldana, D. A.; Starck, L.; Mougin, P.; Rousseau, B.; Pidol, L.; Jeuland, N.; Creton, B. Flash Point and Cetane Number Predictions for Fuel Compounds Using Quantitative Structure Property Relationship (QSPR) Methods. *Energy Fuels* **2011**, *25*, 3900–3908.
- (51) Saldana, D. A.; Starck, L.; Mougin, P.; Rousseau, B.; Ferrando, N.; Creton, B. Prediction of Density and Viscosity of Biofuel Compounds Using Machine Learning Methods. *Energy Fuels* **2012**, 26, 2416–2426.
- (52) Saldana, D. A.; Starck, L.; Mougin, P.; Rousseau, B.; Creton, B. On the rational formulation of alternative fuels: melting point and net heat of combustion predictions for fuel compounds using machine learning methods. *SAR QSAR Environ. Res.* **2013**, *24*, 259–277.
- (53) Hall, C. A. Data-based methods for the screening and design of jet fuels 2024 http://elib.uni-stuttgart.de/handle/11682/15334.
- (54) Hall, C.; Bell, D. C.; Feldhausen, J.; Rauch, B.; Heyne, J. Quantifying isomeric effects: A key factor in aviation fuel assessment and design. *Fuel* **2024**, *357*, No. 129912.
- (55) Das, D. D.; McEnally, C. S.; Kwan, T. A.; Zimmerman, J. B.; Cannella, W. J.; Mueller, C. J.; Pfefferle, L. D. Sooting tendencies of diesel fuels, jet fuels, and their surrogates in diffusion flames. *Fuel* **2017**, 197, 445–458.
- (56) Coffin, J. G. A Study of Airplane Ranges and Useful Loads; National Advisory Committee For Aeronautics, 1920.
- (57) Snijders, T. A.; Melkert, J. A. Using Synthetic Kerosene in Civil Jet Aircraft, SAE Technical Paper Series; SAE, 2008.
- (58) Brem, B. T.; Durdina, L.; Siegerist, F.; Beyerle, P.; Bruderer, K.; Rindlisbacher, T.; Rocci-Denis, S.; Andac, M. G.; Zelina, J.; Penanhoat, O.; Wang, J. Effects of fuel aromatic content on nonvolatile particulate emissions of an in-production aircraft gas turbine. *Environ. Sci. Technol.* **2015**, *49*, 13149–13157.
- (59) Montgomery, M. J.; Das, D. D.; McEnally, C.S.; Pfefferle, L.D. Analyzing the robustness of the yield sooting index as a measure of sooting tendency. *Proc. Combust. Inst.* **2019**, *37*, 911–918.
- (60) Das, D. D.; John, P. C., St.; McEnally, C. S.; Kim, S.; Pfefferle, L. D. Measuring and predicting sooting tendencies of oxygenates, alkanes, alkenes, cycloalkanes, and aromatics on a unified scale. *Combust. Flame* **2018**, *190*, 349–364.
- (61) Wan, K.; Manin, J.; Sim, H. S.; Karathanassis, I. Soot and PAH formation in high pressure spray pyrolysis of gasoline and diesel fuels. *Combust. Flame* **2022**, *241*, No. 112084.
- (62) Leipold, A.; Aptsiauri, G.; Ayazkhani, A.; Bauder, U.; Becker, R.-G.; Berghof, R.; Claßen, A.; Dadashi, A.; Dahlmann, K.; Dzikus, N. et al. *DEPA* 2050-Development Pathways for Aviation up to 2050; DLR, 2021
- (63) Schumann, U.; Heymsfield, A. J. On the Life Cycle of Individual Contrails and Contrail Cirrus. *Meteorol. Monogr.* **2017**, *58*, 3.1–3.24.
- (64) Barrett, S.; Prather, M.; Penner, J.; Selkirk, H.; Balasubramanian, S.; Dopelheuer, A.; Fleming, G.; Gupta, M.; Halthore, R.; Hileman, J.et al. In *Guidance on the use of AEDT Gridded Aircraft Emissions in Atmospheric Models*, A technical note submitted to the US Federal Aviation Administration, Massachusetts Institute of Technology (MIT); Laboratory for Aviation and the Environment, 2010.
- (65) Lee, D. S.; Fahey, D.; Skowron, A.; et al. The contribution of global aviation to anthropogenic climate forcing for 2000 to 2018. *Atmos. Environ.* **2021**, 244, No. 117834.
- (66) Lefebvre, A. H. Fuel Effects on Gas Turbine Combustion—Ignition, Stability, and Combustion Efficiency. *J. Eng. Gas Turbines Power* 1985, 107, 24–37.
- (67) El-Shanawany, M. S.; Lefebvre, A. H. Airblast atomization: effect of linear scale on mean drop size. *J. Energy* **1980**, *4*, 184–189.

- (68) Eckel, G. Large eddy simulation of turbulent reacting multiphase flows, Ph.D. Thesis; University of Stuttgart2018.
- (69) Stöhr, M.; Ruoff, S.; Rauch, B.; Meier, W.; Le Clercq, P. Droplet vaporization for conventional and alternative jet fuels at realistic temperature conditions: Systematic measurements and numerical modeling. *Proc. Combust. Inst.* **2021**, *38*, 3269–3276.
- (70) Ruoff, S.; Stöhr, M.; Rauch, B.; Eckel, G.; Le Clercq, P.; Meier, W.; Aigner, M. Numerical simulation and uncertainty quantification of a generic droplet evaporation validation test case. *Atomization Sprays* **2020**, *30*, 861–879.
- (71) Bell, D. C.; Heyne, J. S.; Won, S. H.; Dryer, F. L. In *The Impact of Preferential Vaporization on Lean Blowout in a Referee Combustor at Figure of Merit Conditions*, Volume 1: Fuels, Combustion, and Material Handling; Combustion Turbines Combined Cycles; Boilers and Heat Recovery Steam Generators; Virtual Plant and Cyber-Physical Systems; Plant Development and Construction; Renewable Energy Systems; ASME, 2018.
- (72) Rock, N.; Chterev, I.; Smith, T.; Ek, H.; Emerson, B.; Noble, D.; Seitzman, J.; Lieuwen, T. In Reacting Pressurized Spray Combustor Dynamics: Part 1 Fuel Sensitivities and Blowoff Characterization, Volume 4A: Combustion, Fuels and Emissions; ASME, 2016.
- (73) Won, S. H.; Rock, N.; Lim, S. J.; Nates, S.; Carpenter, D.; Emerson, B.; Lieuwen, T.; Edwards, T.; Dryer, F. L. Preferential vaporization impacts on lean blow-out of liquid fueled combustors. *Combust. Flame* **2019**, 205, 295–304.
- (74) Stagni, A.; Esclapez, L.; Govindaraju, P.; Cuoci, A.; Faravelli, T.; Ihme, M. The role of preferential evaporation on the ignition of multicomponent fuels in a homogeneous spray/air mixture. *Proc. Combust. Inst.* **2017**, *36*, 2483–2491.
- (75) ASTM D86 Standard Test Method for Distillation of Petroleum Products and Liquid Fuels at Atmospheric Pressure; 2023; Vol. D0086–23A
- (76) Ruoff, S. J.; Rauch, B.; Le Clercq, P.; Aigner, M. Assessment of the Comparability of Droplet Evaporation Fuel Sensitivities between a Unit Test Case and an Aviation Gas Turbine Combustor, AIAA Scitech 2019 Forum; AIAA, 2019.
- (77) Colket, M.; Heyne, J.; Rumizen, M.; et al. Overview of the National Jet Fuels Combustion Program. AIAA J. 2017, 55, 1087–1104
- (78) Boehm, R.; Lohmueller, S.; Andac, G.; Aicholtz, J.; Williams, R.; James, S.; Culbertson, B.; Freeman, G.; Yankowich, P.; Condevaux, J.et al. *Development of Combustion Rules and Tools for the Characterization of Alternative Fuels*, Rept. AFRL-RQ-WP-TR-2013–0223, Phase 2A, 2013.
- (79) Edwards, J. T. Reference Jet Fuels for Combustion Testing. 55th AIAA Aerospace Sciences Meeting. 2017.
- (80) European Union's Horizon 2020 research and innovation programme under grant agreement No 723525 2020 https://cordis.europa.eu/project/id/723525, 06.2017–10.2020. JETSCREEN JET Fuel SCREENing and Optimization.
- (81) International Air Transport Association (IATA) Ramping up SAF through standalone HEFA facilities 2024 https://www.iata.org/en/iata-repository/publications/economic-reports/ramping-up-saf-through-standalone-hefa-facilities/. Accessed: May, 26,2025.
- (82) Lefebvre, A. H.; McDonell, V. G. Atomization and Sprays; CRC Press, 2017.